THE JOURNAL OF PHYSICAL CHEMISTRY B

Article

pubs.acs.org/JPCB

# Metal Cation Dependence of Interactions with Amino Acids: Bond Dissociation Energies of $Rb^+$ and $Cs^+$ to the Acidic Amino Acids and Their Amide Derivatives

P. B. Armentrout,*[,†] Bo Yang,[‡] and M. T. Rodgers*[,‡]

[†]Department of Chemistry, University of Utah, 315 South 1400 E, Room 2020, Salt Lake City, Utah 84112, United States

[‡]Department of Chemistry, Wayne State University, Detroit, Michigan 48202, United States

Supporting Information

**ABSTRACT:** Metal cation–amino acid interactions are key components controlling the secondary structure and biological function of proteins, enzymes, and macromolecular complexes comprising these species. Determination of pairwise interactions of alkali metal cations with amino acids provides a thermodynamic vocabulary that begins to quantify these fundamental processes. In the present work, we expand a systematic study of such interactions by examining rubidium and cesium cations binding with the acidic amino acids (AA), aspartic acid (Asp) and glutamic acid (Glu), and their amide derivatives, asparagine (Asn) and glutamine (Gln). These eight complexes are formed using electrospray ionization and their bond dissociation energies (BDEs) are determined experimentally using threshold collision-induced dissociation with xenon in a guided ion beam tandem mass spectrometer. Analyses of the energy-dependent cross sections include consideration of unimolecular decay rates, internal energy of the reactant ions, and multiple ion-neutral collisions. Quantum chemical calculations are conducted at the B3LYP, MP2(full), and M06 levels of theory using def2-TZVPPD basis sets, with results showing reasonable agreement with experiment. At 0 and 298 K, most levels of theory predict that the ground-state conformers for $M^+$(Asp) and $M^+$(Asn) involve tridentate binding of the metal cation to the backbone carbonyl, amino, and side-chain carbonyl groups, although tridentate binding to the carboxylic acid group and side-chain carbonyl is competitive for $M^+$(Asn). For the two longer side-chain amino acids, Glu and Gln, multiple structures are competitive. A comparison of these results to those for the smaller alkali cations, $Na^+$ and $K^+$, provides insight into the trends in binding energies associated with the molecular polarizability and dipole moment of the side chain. For all four metal cations, the BDEs are inversely correlated with the size of the metal cation and follow the order Asp < Glu < Asn < Gln.

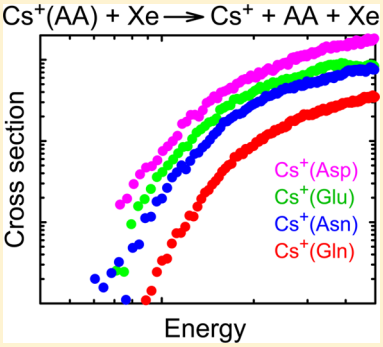


## INTRODUCTION

Sodium and potassium cations are essential nutrients and their enzymatic transfer across cellular membranes is required for homeostasis and cellular function. The heavier alkali metal cations, $Rb^+$ and $Cs^+$, follow the same biological pathways and bind at the same sites as $K^+$,[1,2] but have different transport and accumulation rates.[3−6] Indeed, these kinetic properties allow rubidium and cesium isotopes to be used in imaging of tissue and tumors without severe toxicity.[7] In addition, because atmospheric testing of thermonuclear devices and nuclear reactor accidents have introduced radioactive cesium isotopes into the environment, an understanding of how cesium interacts with biological systems is useful, as reviewed by Gal et al.[8] Despite the potential utility of such studies, the number of systems for which rubidium and cesium cation bond energies are known is much smaller than for sodium and potassium.[8]

Although the interactions of alkali and other cations with all relevant biological systems cannot be explicitly studied, a quantitative examination of a representative set of such interactions, for example with individual amino acids (AAs), can provide substantial insight into more complex systems. This approach creates a "thermodynamic vocabulary" of specific pairwise interactions in small-scale systems[9] that can then be combined to understand systems of greater complexity, such as peptides and even proteins. By working in the gas phase, complications resulting from solvent effects are eliminated and a quantitative measurement of the intrinsic bond strengths between alkali metal cations and peptides can be directly measured. By dealing with relatively small systems, the gas phase experimental information can be directly compared with high level theoretical results. Such comparisons help elucidate subtle features in how metal cation affinities vary with the identity of the metal cation and the variations in peptide side chains. Previously, we have studied the pairwise interactions of all five alkali-metal cations with glycine (Gly),[10−14] proline (Pro),[13−15] serine (Ser),[13,14,16] threonine (Thr),[13,14,16] cysteine (Cys),[14,17] and methionine (Met)[18,19] by examining their threshold collision-induced dissociation (TCID) using guided

**Received:** January 7, 2014
**Revised:** February 7, 2014
**Published:** February 14, 2014





dx.doi.org/10.1021/jp5001754 | J. Phys. Chem. B 2014, 118, 4300−4314

ion beam tandem mass spectrometry (GIBMS). Except for the $Li^+$ complexes, TCID data are also available for histidine (His),[20] phenylalanine (Phe), tyrosine (Tyr), and tryptophan (Trp).[19,21] For the acidic amino acids, aspartic acid (Asp) and glutamic acid (Glu), and their amide derivatives, asparagine (Asn) and glutamine (Gln), TCID data for only the $Na^+$ and $K^+$ complexes are available.[22,23] In all cases, quantitative bond dissociation energies (BDEs) were determined and found to be consistent with theoretical values predicted for the ground-state conformations. In previous work,[9,19,21] these myriad studies are drawn together by the observation that the binding energies for $Na^+$, $K^+$, $Rb^+$, and $Cs^+$ to several amino acids correlate well with the polarizabilities of Gly, Met, and the aromatic amino acids, Phe, Tyr, and Trp. For amino acids containing more polar side chains, the trends with polarizability are retained but appear to be enhanced by the local dipole moment of the polar side chain.[18−20] The present study was initiated in order to explore whether this correlation with polarizability and local dipole moment continues for the heavier alkali metal cations binding to Asp, Asn, Glu, and Gln.

Complementing the thermodynamic study of these complexes are spectroscopic evaluations of their structures using infrared multiple photon dissociation (IRMPD) action spectroscopy. For the four amino acids studied here, the entire sequence of alkali metal cations has been examined using IRMPD with only Asn,[24] with all but $Rb^+$ examined for Gln,[25] and only $Li^+$ and $Cs^+$ examined for Asp and Glu.[26] As for other amino acids, for example, Ser,[27] Thr,[28] Cys,[29] Met,[30] Arg,[31] Trp,[32] Phe,[33] and His,[34] these studies find that the ground geometries of metal cation−amino acid complexes vary with the alkali metal cation identity. Generally, the smaller metal cations, $M^+ = Li^+$ and $Na^+$, bind preferentially in tridentate conformers to the backbone amino, backbone carbonyl, and side-chain heteroatom, whereas spectra for the heavier metal cations, $M^+ = K^+$, $Rb^+$, and $Cs^+$, are more complicated and involve overlapping spectra of several conformers. The results of these spectroscopic studies are compared more thoroughly to the present calculations below.

In the present work, we extend our previous TCID studies to provide the first experimental values for $Rb^+$ and $Cs^+$ binding to the acidic amino acids and their amide derivatives. Absolute BDEs of the $Rb^+$ (AA) and $Cs^+$ (AA) complexes, where AA = Asp, Glu, Asn, and Gln, are measured using TCID in a guided ion beam tandem mass spectrometer. Quantum chemical calculations at several levels of theory are carried out to provide structures, vibrational frequencies, and rotational constants needed for analysis of the TCID data as well as to yield theoretical BDEs for comparison with experiment. The combined experimental and computational studies achieve a quantitative understanding of chelation effects, electron delocalization, inductive effects, and conformational strain on the binding strength of all four amino acids with the rubidium and cesium cations and allow validation of appropriate levels of theory. Comparison with similar results for the smaller alkali metal cations reveals how these effects vary with the size of the metal cation.

## EXPERIMENTAL AND COMPUTATIONAL SECTION

**General Experimental Procedures.** Cross sections for CID of the rubidium and cesium cation−amino acid complexes are measured using the Wayne State University guided ion beam tandem mass spectrometer that has been described in detail previously.[35] Experiments are conducted using an electrospray ionization (ESI) source[36,39] under conditions similar to those described previously.[14,36] Briefly, the ESI is operated using a 50:50 by volume $H_2O$/MeOH solution with $\sim 1 \times 10^{-3}$ M amino acid and $\sim 1 \times 10^{-3}$ M RbCl or CsCl (all chemicals purchased from Sigma-Aldrich). All solutions were acidified at a concentration of $\sim 1 \times 10^{-5}$ M acid, using acetic acid for Asn, Glu, and Gln and HCl for Asp solutions. The electrospray needle was operated near 2 kV, with a flow rate of $\sim 0.8$ μL/min, and a capillary temperature of 105 − 110 °C. All other operating conditions are similar to those used previously. Notably the ESI/ion funnel/radio frequency (rf) hexapole source arrangement used here has been shown to produce ions thermalized to 300 K.[22,36−40]

$Rb^+$(AA) or $Cs^+$(AA) complexes are extracted from the source, focused, accelerated, and mass selected using a magnetic momentum analyzer. The mass-selected ions are decelerated to a well-defined kinetic energy and focused into a rf octopole ion guide that traps the ions radially. The octopole passes through a static gas cell containing xenon, which is used as the collision gas because it is heavy and polarizable, leading to more efficient kinetic to internal energy transfer.[41,42] After collision, the reactant and product ions drift to the end of the octopole where they are extracted and focused into a quadrupole mass filter for mass analysis. The ions are detected with a high voltage dynode, scintillation ion detector[43] and the signal is processed using standard pulse counting techniques. Ion intensities, measured as a function of collision energy, are converted to absolute cross sections as described previously.[44] The uncertainty in relative cross sections is approximately ±5% and that for the absolute cross sections is approximately ±20%. The ion kinetic energy distribution is measured to be Gaussian and has a typical fwhm of 0.2−0.4 eV (lab). Uncertainties in the absolute energy scale are approximately ±0.05 eV (lab). Ion kinetic energies in the laboratory frame are converted to energies in the center-of-mass (CM) frame using $E_{CM} = E_{lab}m/(m+M)$, where $M$ and $m$ are the masses of the ionic and neutral reactants, respectively. All energies herein are reported in the CM frame unless otherwise noted.

**Thermochemical Analysis.** Threshold regions of the CID reaction cross sections are modeled using eq 1[45−48]

$$\sigma(E) = (n\sigma_0/E)\Sigma g_i \int_{E_0-E_i}^{E} P_D(E-\varepsilon)^{n-1} d(\varepsilon) \quad (1)$$

where $\sigma_0$ is an energy-independent scaling factor, $n$ is an adjustable parameter that describes the efficiency of collisional energy transfer,[49] $E$ is the relative kinetic energy of the reactants, $E_0$ is the threshold for dissociation of the ground electronic and rovibrational state of the reactant ion at 0 K, $\tau$ is the experimental time for dissociation ($\sim 10^{-4}$ s), $\varepsilon$ is the energy transferred from translation during the collision, and $E^*$ is the internal energy of the energized molecule (EM) after the collision, that is, $E^* = \varepsilon + E_i$. The summation is over the rovibrational states of the reactant ions, $i$, where $E_i$ is the excitation energy of each state and $g_i$ is the fractional population of those states ($\sum g_i = 1$). The Beyer−Swinehart algorithm[50−52] is used to evaluate the number and density of the rovibrational states and the relative populations $g_i$ are calculated for a Maxwell−Boltzmann distribution at 300 K.

The term $P_D$, the dissociation probability, is given by $P_D = 1 - e^{-k(E^*)\tau}$, where $k(E^*)$ is the unimolecular rate constant for dissociation of the energized molecule. This is defined by


dx.doi.org/10.1021/jp5001754 | J. Phys. Chem. B 2014, 118, 4300−4314

Rice−Ramsperger−Kassel−Marcus (RRKM) theory, as in eq 2[53,54]

$$k(E^*) = dN^{\dagger}_{vr}(E^* - E_0)/h\rho_{vr}(E^*) \quad (2)$$

where $d$ is the reaction degeneracy (determined using rotational symmetry numbers), $N^{\dagger}_{vr}(E^* - E_0)$ is the sum of rovibrational states of the transition state (TS) at an energy $E^* - E_0$, and $\rho_{vr}(E^*)$ is the density of states of the energized molecule (EM) at the available energy, $E^*$. These rate constants allow kinetic shifts to be modeled as discussed below.[47,55]

Several effects that obscure the interpretation of the data must be accounted for during data analysis in order to produce accurate thermodynamic information. These effects include multiple collisions, kinetic shifts, and energy broadening resulting from the thermal motion of the neutral collision gas and the kinetic energy distribution of the reactant ion. These effects are handled as detailed in previous work.[23] For all eight systems, data at nominal Xe pressures of 0.2, 0.1, and 0.05 mTorr were obtained in duplicate and used to extrapolate to zero pressure, corresponding to truly single collision conditions. For a couple of systems, $Cs^+$(Asp), $Cs^+$(Glu), and $Cs^+$(Asn), additional sets of data were obtained. In the former case, the original data set had a cross section that differed in shape from that of other systems, whereas the repeated data acquisition yielded a cross section shape that paralleled other systems and hence was used exclusively. For $Cs^+$(Glu), both sets of data agreed with only differences in absolute magnitude observed (~30%). For $Cs^+$(Asn), two of three data sets agreed well and their average results are reported below. (The third data set shows evidence of hot ions and was therefore discarded.) As discussed previously, kinetic shifts are estimated by the incorporation of RRKM theory, as shown in eq 1, which requires sets of rovibrational frequencies for the EM and TS. These molecular parameters are taken from the quantum chemical calculations detailed in the next section. Because the metal−ligand interactions in the $M^+$(AA) complexes are mainly electrostatic, the most appropriate model for the TS for dissociation of the intact ligand is a loose association of the ion and neutral ligand fragments in a phase space limit (PSL).[47,55] The appropriateness of this assumption for multidentate ligands has been verified previously for crown ethers[39,40,56−58] and small peptides,[37] and the sodiated and potassiated complexes of the four amino acids studied here.[22,23]

Model cross sections calculated using eq 1 are convoluted with the kinetic energy distribution of both reactants,[44,59] then compared to the zero pressure extrapolated reaction cross sections[60] using a nonlinear least-squares routine allowing parameters for $\sigma_0$, $n$, and $E_0$ to be optimized. The uncertainty associated with $E_0$ is estimated from the range of threshold values determined from different data sets with variations in the parameter $n$, ±10% variations in vibrational frequencies, changes in the experimental time for dissociation by factors of two, and the uncertainty of the absolute energy scale, ±0.05 eV (lab). All other details regarding data interpretation and necessary assumptions in the modeling have been fully described previously.[22,23]

In deriving the final experimental BDEs at 0 K, two assumptions are made. First, we assume that there is no activation barrier in excess of the reaction endothermicity for the loss of the AA ligand, which is generally true for ion−molecule reactions and for heterolytic noncovalent bond dissociations such as those considered here.[61] Second, the measured threshold $E_0$ values for dissociation are from ground state reactant to ground state ion and neutral ligand products. Given the relatively long experimental time frame (~$10^{-4}$ s), dissociating products should be able to rearrange to their low-energy conformations after collisional excitation.

**Computational Details.** All theoretical calculations were performed using Gaussian09.[62] Ground-state conformers of the four amino acids calculated at the B3LYP/6-311+G(d,p) level of theory have been described previously[22] and, in all cases, were reoptimized here at the B3LYP/def2-TZVPPD level of theory.[63,64] This level of theory is needed because it provides accurate BDEs for complexes of the larger alkali cations.[13,14,19] Previous studies have shown that a HW*/6-311+G(d,p) basis set, where HW* indicates that Rb and Cs were described using the effective core potentials (ECPs) and valence basis sets of Hay and Wadt[65] (equivalent to the LANL2DZ basis set) with a single d polarization function added,[66] is inadequate to describe the energetics of $Rb^+$ and $Cs^+$ complexes.[13,14,17,20,58] The def2-TZVPPD basis set[67,68] is a balanced basis set on all atoms at the triple-ζ level including polarization and diffuse functions and uses ECPs on rubidium and cesium developed by Leininger et al.[69] The def2-TZVPPD basis set was obtained from the EMSL basis set exchange library.[70,71] Likely low-energy conformers of Asp, Asn, Glu, and Gln complexed with $Rb^+$ and $Cs^+$ utilized those structures previously found for $K^+$(AA) as starting points for the present work.[23] For all complexes and free AAs, geometry optimizations and vibrational frequencies were calculated at the B3LYP/def2-TZVPPD level, with zero point energies being scaled by 0.989.[72] Single point energies at this level as well as the M06/def2-TZVPPD[73] and MP2(full)/def2-TZVPPD[74] levels using the B3LYP geometries were also calculated. Basis set superposition errors (BSSE) corrections at the full counterpoise (cp) level[75,76] were applied in all cases and ranged from <0.7 kJ/mol for the DFT calculations to 13−22 kJ/mol for $Rb^+$ complexes and 7−14 kJ/mol for $Cs^+$ complexes for the MP2(full) results. Previous work indicates that the large BSSE corrections for MP2 can be attributed primarily to a decrease in the energy of the metal cation.[19] Previous experience with complexes of $Cs^+$ finds that cp corrections for the MP2(full) results are needed in order to provide reasonable agreement with experiment.[14,19] Here, we find that without cp corrections, the MP2 values for both $Rb^+$ and $Cs^+$ complexes greatly exceed experimental values.

In previous work on complexes of $Rb^+$ and $Cs^+$ with other amino acids, geometries were also calculated at the M06 and M06-2X levels.[19] The former results provided very similar geometries and relative energies as the M06//B3LYP results with an average difference of 1.1 ± 1.0 kJ/mol. Results calculated using the M06-2X approach, designed for main group elements in particular but not transition metals,[73] yielded bond energies 6−14 kJ/mol higher in energy than the M06 results, making the M06-2X results in the poorest agreement with experiment of all levels of theory examined. Here, the lowest energy structures for each complex were reoptimized at the M06/def2-TZVPPD level, but again very similar geometries and relative energies compared to the B3LYP/def2-TZVPPD results were obtained.

For $Cs^+$(Asp), $Cs^+$(Glu), and $Cs^+$(Gln), vibrational frequencies and intensities were calculated using the harmonic oscillator approximation and analytical derivatives of the energy-minimized Hessian calculated at the B3LYP/def2-TZVPPD level of theory. For comparison to


dx.doi.org/10.1021/jp5001754 | J. Phys. Chem. B 2014, 118, 4300−4314

IRMPD spectra, frequencies were scaled by 0.98 as this scaling factor leads to good agreement between calculated and experimentally well-resolved peaks. Calculated vibrational frequencies are broadened using a 20 (Asp and Glu complexes) or 30 (Gln complex) $cm^{-1}$ fwhm Gaussian line shape for comparison with experimental spectra.

**Conversion from 0 to 298 K and Excited Conformers.** Relative energies calculated at 0 K are converted to free energies at 298 K using the rigid rotor/harmonic oscillator approximation. The needed rotational constants and vibrational frequencies are calculated at the B3LYP/def2-TZVPPD level. The relative $\Delta G_{298}$ excitation energies reported below are comparable to the analogous differences in the $\Delta H_0$ values with differences not exceeding 5 kJ/mol (and most differences less than 2 kJ/mol). The experimental 0 K bond energies are also converted to $\Delta H_{298}$ and $\Delta G_{298}$ values, with uncertainties estimated by varying most vibrational frequencies by ±10% along with 2-fold variations in the metal cation-AA frequencies.

## RESULTS

**Cross Sections for Collision-Induced Dissociation.** Experimental kinetic energy-dependent cross sections were obtained for the interaction of Xe with $M^+$(AA), where $M^+$ = $Rb^+$ and $Cs^+$ and AA = Asp, Glu, Asn, and Gln. Figure 1 compares results for $Rb^+$ (part a) and $Cs^+$ (part b). Data shown are zero-pressure extrapolated results because, although the pressure dependence of these cross sections is small in all cases, there is a measurable effect on the thresholds. In all cases, the simple collision-induced dissociation (CID) reactions, eq 1, are the only dissociation pathway observed.

$$M^+(AA) + Xe \rightarrow M^+ + AA + Xe \quad (1)$$

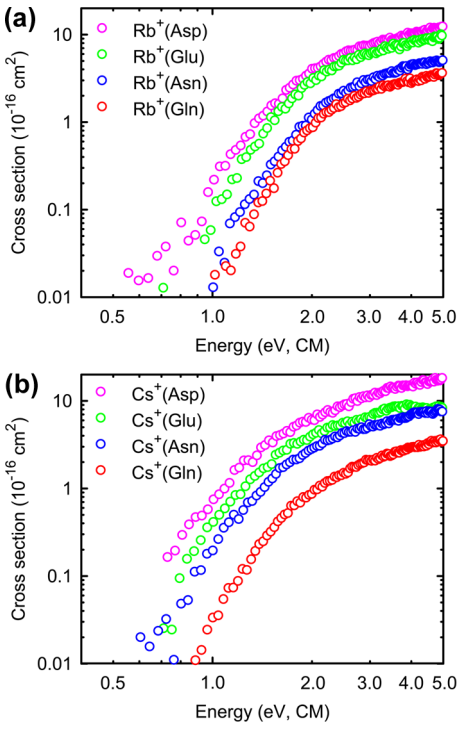


**Figure 1.** Zero-pressure extrapolated cross sections for collision-induced dissociation of $Rb^+$(AA) (part a) and $Cs^+$(AA) (part b), where AA = Asp, Glu, Asn, and Gln with xenon as a function of kinetic energy in the center-of-mass frame.

Loss of $H_2O$ and $NH_3$ was specifically looked for as one or both pathways were observed for $Na^+$(Asn), $Na^+$(Glu), $Na^+$(Gln), and $K^+$(Gln).[22,23] The failure to observe these channels here can be attributed to the weaker binding of the metal cation to the amino acid, such that reaction 1 is both energetically and entropically favored over the more complex elimination reactions.[77,78] Figure 1 demonstrates that the thresholds increase in the order Asp, Glu, Asn, and Gln for both metal cations along with a commensurate decrease in the absolute magnitude of the cross sections. Thus, the relative order of the binding among these four amino acids is unambiguous.

The zero pressure extrapolated cross sections for all eight $M^+$(AA) systems were analyzed using the models of eq 1 (lifetime effects included) and without lifetime effects (eq 1 with $P_D$ set to unity). Figure 2 shows a representative data set for $Cs^+$(Gln), and Figure S1 shows results for all eight $M^+$(AA) systems. It can be seen in both figures that the experimental cross sections are reproduced by eq 1 (including lifetime effects) over a large range of energies (>3 eV) and cross section magnitudes (>2 orders of magnitude). In all eight systems, analyses were performed using molecular parameters for all structures that theory indicates could be the ground state (see Discussion). Table 1 lists the optimized fitting parameters of eq 1 for a variety of combinations of reactant and product conformations. Combinations with threshold energy differences less than 0.02 eV are not included but can be found in Table S1 of the Supporting Information. Comparison of threshold energies obtained with and without lifetime effects shows that kinetic shifts occur in all systems, ranging from 0.12 eV for $Cs^+$(Asp), the most weakly bound system, to 0.42 eV for $Rb^+$(Gln), the most strongly bound system. The values of the entropy of activation at 1000 K, $\Delta S^{\ddagger}_{1000}$, are also listed in Tables 1 and S1 and give some idea of the looseness of the transition states. Varying from 16 to 63 J/K·mol, these values are in the range suggested by Lifshitz[79] as corresponding to simple bond cleavage dissociations. Given that the TSs are assumed to lie at the centrifugal barrier for the association of $M^+$ + AA, this is an expected result.

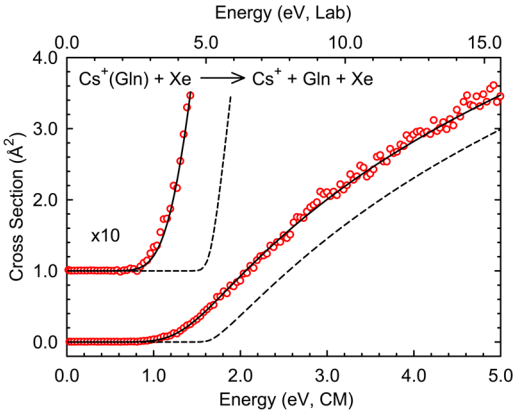


**Figure 2.** Cross section for collision-induced dissociation of $Cs^+$(Gln) with xenon as a function of kinetic energy in the center-of-mass frame (lower *x*-axis) and the laboratory frame (upper *x*-axis). Solid lines show the best fit to the data using the model of eq 1 convoluted over the neutral and ion kinetic and internal energy distributions. Dashed lines show the model cross section in the absence of experimental kinetic energy broadening for reactant ions with an internal energy of 0 K. The data and models are also shown expanded by a factor of 10 and offset from zero.


dx.doi.org/10.1021/jp5001754 | J. Phys. Chem. B 2014, 118, 4300−4314

Table 1. Fitting Parameters of Eq 1 and Entropies of Activation at 1000 K for CID of $Rb^+$(AA) and $Cs^+$(AA) for AA = Asp, Glu, Asn, and Gln[a]

| reactant | $M^+$(AA)/AA structures | $\sigma_0$ | $n$ | $E_0$ (no RRKM) (eV) | $E_0$(PSL)[b] ( eV) | $\Delta S^{\ddagger}_{1000}$ (J/K·mol) |
|---|---|---|---|---|---|---|
| $Rb^+$(Asp) | [N,CO,CO]/N1 | 10.2 (0.4) | 1.3 (0.1) | 1.49 (0.07) | 1.31 (0.07) | 39 (2) |
| $Rb^+$(Glu) | [N,CO,CO]/N1 | 9.8 (1.7) | 1.2 (0.1) | 1.66 (0.08) | 1.35 (0.08) | 40 (2) |
| | [N,CO,CO]/N3 | | | | $+0.03_1$ | 58 (2) |
| | [N,CO,CO]/N4 | | | | $+0.04_1$ | 63 (2) |
| | [CO,CO]cgtgtt/N1 | | | | $-0.02_1$ | 32 (2) |
| $Rb^+$(Asn) | [N,CO,CO]/N1 | 4.9 (0.6) | 1.3 (0.1) | 1.74 (0.07) | 1.43 (0.07) | 30 (2) |
| | [N,CO,CO]/N2 | | | | $+0.02_9$ | 44 (2) |
| $Rb^+$(Gln) | [COOH,CO]cgg$_+$g_t/N1 | 4.4 (0.6) | 1.1 (0.1) | 1.88 (0.07) | 1.46 (0.07) | 37 (2) |
| | [COOH,CO]cgg$_+$g_t/N3 | | | | $-0.06_6$ | 18 (2) |
| | [COOH,CO]cgg$_+$g_t/N4 | | | | $-0.08_0$ | 16 (2) |
| | [COOH,CO]cgg_g$_+$t/N1 | | | | $+0.04_2$ | 49 (2) |
| | [CO,CO]cgggt/N1 | | | | $+0.03_4$ | 46 (2) |
| $Cs^+$(Asp) | [N,CO,CO]/N1 | 11.8 (1.1) | 1.5 (0.1) | 1.25 (0.07) | 1.13 (0.07) | 36 (2) |
| | [COOH$_s$]/N1 | | | | $-0.03_8$ | 20 (2) |
| $Cs^+$(Glu) | [N,CO,CO]/N1 | 6.5 (1.4) | 1.5 (0.2) | 1.33 (0.07) | 1.14 (0.07) | 35 (2) |
| | [N,CO,CO]/N3 | | | | $+0.02_0$ | 54 (2) |
| | [N,CO,CO]/N4 | | | | $+0.02_6$ | 58 (2) |
| $Cs^+$(Asn) | [N,CO,CO]/N1 | 4.7 (2.4) | 1.5 (0.2) | 1.38 (0.07) | 1.20 (0.07) | 27 (2) |
| $Cs^+$(Gln) | [COOH,CO]cgg$_+$g_t/N1 | 2.8 (0.4) | 1.4 (0.1) | 1.61 (0.07) | 1.33 (0.07) | 44 (2) |
| | [COOH,CO]cgg$_+$g_t/N3 | | | | $-0.05_3$ | 26 (2) |
| | [COOH,CO]cgg$_+$g_t/N4 | | | | $-0.06_8$ | 24 (2) |
| | [CO,CO]cgtgt/N1 | | | | $-0.02_3$ | 35 (2) |

[a]Uncertainties (1 std dev) in parentheses. [b]Values for alternative conformations list shifts from the baseline $E_0$ value.

The effect of having different conformers populating the $M^+$(AA) cation beams was investigated thoroughly. In addition, the possibility that different conformers of the AA product were formed was also considered. The only fitting parameter of eq 1 to change significantly is the threshold energy, $E_0$. For the shorter side-chain Asp and Asn amino acids, differences in the threshold energies among different $M^+$(AA) and AA conformers are ≤0.02 eV, Tables 1 and S1, except for $Cs^+$(Asp) [$COOH_s$] (see definition of nomenclature in the next section) where the shift is 0.04 eV and dissociation of $Rb^+$(Asn) to the N2 conformer of Asn (0.03 eV shift). These differences are well within the overall experimental uncertainty of any individual measurement, ~0.07 eV. For Glu and Gln, the shifts associated with different $M^+$(AA) conformers range from 0.00 to 0.05 eV, whereas those for different conformers of the AA product are 0.00 to 0.08 eV, still less than or comparable to the experimental uncertainty. These shifts occur because of differences in the kinetics of dissociation, as can also be seen by examining the entropies of activation. Lower entropies of activation are directly correlated with lower thresholds because there is a larger kinetic shift associated with the more restricted dissociation process. Overall, as indicated by IRMPD results reviewed below,[24−26] multiple conformations of the $M^+$(AA) complexes are probably formed in the source, but the bond energies obtained experimentally are largely insensitive to this variation because the energy content of the different conformers (both before and after collision) is approximately equal and differences in the unimolecular dissociation kinetics are small. In contrast, the dissociation behavior will be dominated by formation of the entropically most favorable AA product conformer as long as it lies within a couple of kJ/mol of the ground conformer. This conclusion was verified by direct examination of the calculated RRKM rates for these dissociations. Specific considerations for each system are discussed further in the sections below.

**Theoretical Results for AA.** Structures of the four neutral amino acids were calculated using the B3LYP/def2-TZVPPD approach with single point energies calculated at the B3LYP, M06, and MP2(full) levels including zero point energy corrections. The results obtained here are very similar to those calculated at the R/6-311+G(2d,2p)//B3LYP/6-311+G(d,p) level, where R = B3LYP, B3P86, and MP2(full).[22] These results are summarized in Table 2, where the conformers are identified by designating the approximate dihedral angles of the side chains (c for cis, <50°; t for trans, >130°; and g for gauche, all intermediate angles) with "+" and "−" subscripts to indicate the sign on gauche angles when needed to differentiate conformers. For the two shorter side-chain amino acids, Asp and Asn, the angle designations start at the C-terminus and specify ∠HOCC, ∠OCCC, ∠CCCC, and ∠CCCX, where X is the hydroxyl oxygen or amide nitrogen of the side chain, with the ∠CCOH orientation of the side-chain carboxylic acid included as the last designation for Asp. For the longer side-chain amino acids, Glu and Gln, there is an additional ∠CCCC angle, listed before ∠CCCX, and again Glu includes the ∠CCOH orientation of the side-chain. For conciseness later on, we also designate these conformers using a simple Nx nomenclature as well (see below). Results were also obtained with M06 theory being used for geometry optimizations, that is, at the R/def2-TZVPPD//M06/def2-TZVPPD levels, but largely parallel those listed in Table 2. Table S2 of the Supporting Information contains the energetic details of these calculations.

For aspartic acid, the ctttt (N1), ctgtt (N2), and tcgtt (N4) conformers are either the ground state or within 1 kJ/mol of the ground state at some level of theory. The tgtcc (N3) conformer (mislabeled as cctgt previously)[22] is generally higher in energy at all levels. For asparagine, the ctgg (N1) conformer is the clear ground state with other conformers lying 2−10 kJ/mol higher in energy. The ground state for glutamic


dx.doi.org/10.1021/jp5001754 | J. Phys. Chem. B 2014, 118, 4300−4314

**Table 2. Relative Free Energies (kJ/mol) at 0 K for Low-Energy Structures of Asp, Asn, Glu, and Gln Calculated at the Indicated Levels of Theory[a]**

| | 6-311+G(2d,2p)[b] | | | def2-TZVPPD[c] | | |
|---|---|---|---|---|---|---|
| structure | B3LYP | B3P86 | MP2(full) | B3LYP | M06 | MP2(full) |
| Asp | | | | | | |
| ctttt (N1) | **0.0** | **0.0** | 1.4 | **0.0** | 0.7 | 1.6 |
| ctgtt (N2) | 2.0 | 1.7 | **0.0** | 1.6 | **0.0** | **0.0** |
| tgtcc (N3) | 3.6 | 3.4 | 4.3 | 3.6 | 7.0 | 4.4 |
| tcgtt (N4) | 4.5 | 7.5 | 0.4 | 4.4 | 1.8 | 1.4 |
| Asn | | | | | | |
| ctgg (N1) | **0.0** | **0.0** | **0.0** | **0.0** | **0.0** | **0.0** |
| cttt (N2) | 2.2 | 3.2 | 7.6 | 2.3 | 4.1 | 8.2 |
| cggt (N3) | 3.1[d] | 4.9[d] | 9.5[d] | 3.0 | 6.4 | 10.1 |
| cgtg (N4) | 4.0[d] | 5.1[d] | 8.7[d] | 4.2 | 7.4 | 8.8 |
| Glu | | | | | | |
| ctggtt (N1) | 0.7 | **0.0** | 1.3 | 1.1 | **0.0** | **0.0** |
| cgtgtt (N2) | 0.9 | 0.6 | 3.5 | 1.0 | 1.1 | 2.2 |
| tgtgtt (N3) | 0.3 | 4.0 | **0.0** | 0.1 | 0.1 | 0.3 |
| tgtttt (N4) | **0.0** | 5.0 | 2.7 | **0.0** | 1.5 | 2.9 |
| Gln | | | | | | |
| ctggt (N1) | **0.0** | **0.0** | 2.5 | **0.0** | 0.7 | 2.2 |
| cgtgt (N2) | 1.8 | 1.8 | 6.5 | 1.4 | 3.5 | 6.5 |
| $cg_+ggg$ (N3) | 2.1 | 2.5 | **0.0** | 2.0 | **0.0** | **0.0** |
| $cg_-ggg$ (N4) | 3.8 | 4.8 | 1.9 | 2.8 | 3.7 | 2.9 |

[a]Ground state conformers in bold. [b]Values from ref 22. [c]This work. [d]Values for the N3 and N4 conformers of Asn were inadvertently switched in ref 22.

acid varies according to the level of theory with ctggtt (N1) being favored by B3P86, M06, and MP2(full)/def2-TZVPPD calculations, whereas MP2(full)/6-311+G(2d,2p) calculations favor tgtgtt (N3) and B3LYP calculations indicate tgtttt (N4) as the ground conformer. Even the cgtgtt (N2) conformer lies within 1 kJ/mol of the ground state at several levels of theory (and is the B3LYP/def2-TZVPPD//M06/def2-TZVPPD ground state, Table S2). Similar diversity is found for glutamine with ctggt (N1) generally being favored by B3LYP and B3P86 calculations and $cg_+ggg$ (N3) being favored by MP2(full) and M06 calculations. The other two conformers, cgtgt (N2) and $cg_-ggg$ (N4) are consistently higher in energy, by 1.4−6.5 kJ/mol (with the exception that N2 is the B3LYP/def2-TZVPPD//M06/def2-TZVPPD ground state, Table S2).

**Theoretical Results for $M^+$(AA) and Comparison to IRMPD Spectra.** Structures of the complexes of the four neutral amino acids with $Rb^+$ and $Cs^+$ experimentally studied here were calculated as described above. Figure 3 shows the possible ground-state conformers for the cesiated complexes. The nomenclature adopted here identifies the binding sites of the metal ion in brackets: the backbone amino nitrogen (N), the backbone or sidechain carbonyl (CO), both oxygens of the backbone carboxylic acid (COOH), both oxygens of a backbone zwitterionic carboxylate ($CO_2^-$), or both oxygens of the side-chain carboxylic acid [$COOH_s$]. This is followed by the same designation of dihedral angles of the AA noted above.

Table 3 provides energetic information for the key low-lying conformers of the $M^+$(AA) complexes as both 0 and 298 K free energies, with the latter providing the basis for which structures might be populated experimentally. Tables S3 and S4 of the Supporting Information list energetic and geometric information, respectively, on all conformers located. We also optimized the geometries of several low-energy conformers for each complex at the M06/def2-TZVPPD level, with relative energies compared to the B3LYP geometries in Table S5. The M06 geometries lead to relative energies in general agreement with those from B3LYP geometries, with most ground states being the same and relative energies generally within 1 kJ/mol, but differences of up to 5 kJ/mol are observed. Previous theoretical work on these systems has been reported in conjunction with IRMPD experimental studies for Asn and Gln,[22,23,25] whereas for Asp and Glu, only the cesium complexes have been explored.[25,26] Relative energies from these previous studies are included in Tables 3 and S3. Related work includes the structures of the $Na^+$(AA) and $K^+$(AA) complexes with all four amino acids.[22,23,25] As the present calculations parallel many of these previous results, only an abbreviated discussion is provided here.

IRMPD spectra of aspartic and glutamic acids with alkali metal cations are available only for $M^+ = Li^+$ and $Cs^+$. In parallel with other amino acids having oxygen containing side chains (Ser, Thr),[27,28] the spectra for complexes of Asp and Glu with $Li^+$ can be assigned to the tridentate [N,CO,CO] conformers. For $Cs^+$(Asp) and $Cs^+$(Glu), the spectra are very similar, suggesting that these complexes have similar structures. $Cs^+$(Asp) was assigned largely to a [COOH,CO] structure, with possible contributions from [N,CO,CO] and [CO,CO] conformers. In contrast, $Cs^+$(Glu) was assigned to likely contributions from all three of these conformers: [CO,CO], [COOH,CO], and [N,CO,CO]. One of the reasons for the disparity in assignments compared to $Cs^+$(Asp) is that the calculated $Cs^+$(Glu) [COOH,CO] structure no longer reproduced an intense band observed at ~1140 $cm^{-1}$, attributed to an OH bend, because this intensity is dispersed by coupling this motion with CH and NH twists. As discussed below, the present calculations remove this discrepancy in assignments.

IRMPD spectra for $M^+$(Gln), where $M^+ = Li^+$, $Na^+$, $K^+$, and $Cs^+$, are available.[25] Relative intensities of several bands evolve with the metal cations, but most of the bands persist for all four metal cations. A notable difference between the spectrum of $Cs^+$(Gln) and those for the other three metal cations is the lower relative intensity of the carbonyl stretch for the carboxylic acid group. For the smaller alkali cations, Bush et al. assign the predominant structure as [N,CO,CO] with additional contributions from [CO,CO] and possibly [COOH,CO] as the metal gets larger. For $Cs^+$(Gln), the authors rule out contributions from zwitterionic structures (their calculated ground state at the B3LYP level and the 0 K MP2 ground state, Table 3) and attribute the observed spectrum to [COOH,CO] and [N,CO,CO] (their MP2 ground state at 298 K) structures.

**Experimental and Theoretical Results for $M^+$(Asp).** At 0 K, all levels of theory used here indicate that the aspartic acid complexes have a tridentate binding pattern, [N,CO,CO], Table 3. At 298 K, this remains the ground state for $Rb^+$(Asp) and for both M06 and MP2(full) calculations for $Cs^+$(Asp), but the B3LYP results indicate that the $Cs^+$(Asp) [$COOH_s$] conformer lies 0.3 kJ/mol lower in energy. The [COOH,CO] structure is low-lying, 2−7 kJ/mol above the ground state, with all other conformers lying >9 kJ/mol higher at the M06 and MP2(full) levels, Table S3. These higher-lying conformers include two zwitterionic structures, [$CO_2^-$]ctgtt and [$CO_2^-$]cgttt, and their charge solvated analogues, [COOH]ctgtt and [COOH]cgttt. B3LYP results suggest that two [CO,CO] conformers and the [COOH]ctgtt conformer are also low-lying, 5−9 (2−4) kJ/mol above the ground state


dx.doi.org/10.1021/jp5001754 | J. Phys. Chem. B 2014, 118, 4300−4314

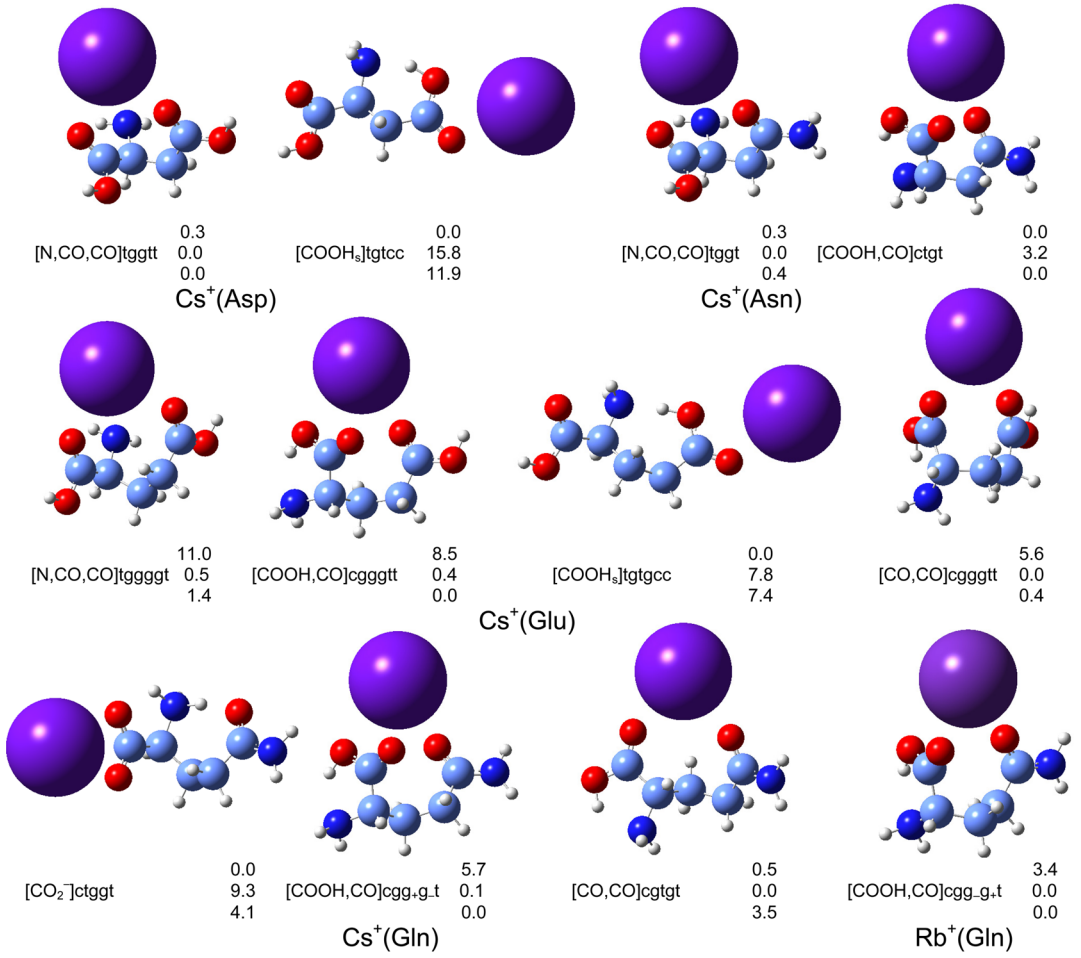


**Figure 3.** Low-energy structures of $Cs^+$(AA) calculated at the B3LYP/def2-TZVPPD level. Relative free energies at 298 K in kJ/mol calculated at the B3LYP, M06, and MP2(full) (top to bottom) levels of theory using the def2-TZVPPD basis sets are shown.

for $Rb^+$ ($Cs^+$). It is notable that our B3LYP results do not parallel those from O'Brien et al. for $Cs^+$(Asp), performed at the B3LYP/CRENBL/6-31++G(d,p) level of theory.[26] They found a ground state of [COOH,CO] with [$COOH_s$] lying only 2 (2) kJ/mol higher at 0 (298) K and [N,CO,CO] lying 7 (10) kJ/mol higher. The [CO,CO]ctg$_+$g$_+$t and [$CO_2^-$]ctgtt conformers were also located by O'Brien et al. but lie 11 (18) and 11 (14) kJ/mol above the ground state. Neither the [CO,CO]ctg_g_t nor the [COOH]ctgtt, [$CO_2^-$]cgttt, and [COOH]cgttt conformers, were located by O'Brien et al., even though the former lies below the [CO,CO]ctg$_+$g$_+$t conformer that they did describe.

IRMPD studies of $Cs^+$(Asp) were concluded by O'Brien et al.[26] to be most consistent with the [COOH,CO] structure, with contributions from [CO,CO]ctg$_+$g$_+$t and [N,CO,CO] being possible. The [$COOH_s$] structure is inconsistent with the observed spectrum. These assignments are nicely consistent with the present M06 and MP2(full) relative energetics but are inconsistent with the B3LYP and previous calculations that find the [$COOH_s$] structure to be low-lying. In light of the present results, a re-examination of the spectrum shows three strong bands at ~1150, 1400, and 1780 $cm^{-1}$. The [$COOH_s$] structure exhibits a medium intensity band at ~1500 $cm^{-1}$ that is inconsistent with experiment (in agreement with the conclusions of O'Brien et al.).[26] Both [N,CO,CO] and [COOH,CO] structures exhibit similar bands (previous and present calculations yield very similar IR spectra), but the band at 1780 $cm^{-1}$ is too broad in the [COOH,CO] spectrum, and the observed intensity of the 1400 $cm^{-1}$ band lies in between that of the two predicted spectra. Interestingly, the average of the [N,CO,CO] and [COOH,CO] spectra yields a result in good agreement with the observed spectrum in positions, shapes, and relative intensities of all bands, as shown in Figure S2. This suggests that the relative energies of these two conformers are similar with other conformers not contributing appreciably, a result most consistent with the present MP2(full) results where an equilibrium distribution at 298 K would have 66% [N,CO,CO], 27% [COOH,CO], and <7% of all other conformations.

In the analysis of the TCID data, results were interpreted assuming the [N,CO,CO] ground state for $Rb^+$(Asp) and both [N,CO,CO] and [COOH,CO] conformers for $Cs^+$(Asp), Table 1. The thresholds obtained for the latter differ by only 0.005 eV, Table S1, in concert with very similar $\Delta S^{\dagger}_{1000}$ values. If the $Cs^+$(Asp) [$COOH_s$] B3LYP ground conformer is assumed, the threshold obtained shifts down by 0.04 eV, Table 1, but the $\Delta S^{\dagger}_{1000}$ value is much lower than for the other two conformers. As there is no evidence for this species in the IRMPD spectra, this species is presumed not to contribute. Dissociations to both the N1 and N2 conformers of Asp were checked and differed from one another by less than 0.01 eV for both metal cations, with N1 having the larger $\Delta S^{\dagger}_{1000}$ value. Likewise, interpretation assuming dissociation to the N3 and N4 conformers of Asp yields thresholds and $\Delta S^{\dagger}_{1000}$ values


dx.doi.org/10.1021/jp5001754 | J. Phys. Chem. B 2014, 118, 4300−4314

**Table 3. Relative Free Energies (kJ/mol) at 0 (298) K for Low-Energy Structures of Rubidium and Cesium-Cation Bound Asp, Asn, Glu, and Gln[a]**

| | relative energies (kJ/mol)[b] | | | |
|---|---|---|---|---|
| structure | B3LYP | M06 | MP2(full) | literature |
| $M^+$(Asp) | | | | B3LYP/CRENBL[c] |
| [N,CO,CO]tggtt | **0.0** (**0.0**) | **0.0** (**0.0**) | **0.0** (**0.0**) | |
| | **0.0** (0.3) | **0.0** (**0.0**) | **0.0** (**0.0**) | 7 (10) |
| [COOH,CO]ctgtt | 5.9 (4.8) | 7.2 (6.0) | 6.4 (5.2) | |
| | 2.2 (1.7) | 4.7 (4.0) | 2.9 (2.2) | **0** (**0**) |
| [$COOH_s$]tgtcc | 9.0 (5.2) | 22.0 (18.3) | 21.4 (17.6) | |
| | 4.2 (**0.0**) | 20.2 (15.8) | 16.3 (11.9) | 2 (2) |
| $M^+$(Asn) | | | | B3P86/def2[d] |
| [N,CO,CO]tggt | **0.0** (**0.0**) | **0.0** (**0.0**) | **0.0** (**0.0**) | 2.4 (2.3) |
| | 0.6 (0.3) | **0.0** (**0.0**) | 0.7 (0.4) | 6.9 (6.3) |
| [COOH,CO]ctgt | 2.7 (2.7) | 4.8 (4.8) | 2.3 (2.3) | **0.0** (**0.0**) |
| | **0.0** (**0.0**) | 2.8 (3.2) | **0.0** (**0.0**) | **0.0** (**0.0**) |
| $M^+$(Glu) | | | | B3LYP/CRENBL[c] |
| [N,CO,CO]tggg$_+$g_t | 3.0 (5.0) | **0.0** (**0.0**) | **0.0** (**0.0**) | |
| | 5.6 (11.0) | **0.0** (0.5) | 1.2 (1.4) | 13 (12) |
| [COOH,CO]cgggtt | 2.6 (5.0) | 1.3 (1.7) | 0.2 (0.7) | |
| | 3.3 (8.5) | 0.1 (0.4) | **0.0** (**0.0**) | |
| [CO,CO]cgggtt | 1.6 (2.0) | 2.7 (1.1) | 3.5 (1.9) | |
| | 2.3 (5.6) | 1.6 (**0.0**) | 2.3 (0.4) | 1 (4) |
| [CO,CO]cgtgtt | **0.0** (**0.0**) | 4.3 (2.3) | 8.0 (6.0) | |
| | 1.0 (3.7) | 4.2 (2.0) | 7.7 (5.2) | |
| [COOH,CO]ctccgt | 14.4 (17.4) | 13.2 (14.2) | 8.4 (9.4) | |
| | 14.6 (20.2) | 11.0 (11.7) | 7.4 (7.8) | 9 (12) |
| [$CO_2^-$]cgtgtt | 0.2 (1.9) | 11.6 (11.4) | 8.5 (8.3) | |
| | 0.7 (5.1) | 12.5 (12.0) | 9.7 (8.9) | **0** (**0**) |
| [$CO_2^-$]ctggtt | 0.5 (2.0) | 14.5 (14.1) | 12.2 (11.8) | |
| | **0.0** (4.8) | 10.1 (10.0) | 5.7 (5.3) | |
| [$COOH_s$]tgtgcc | 2.2 (2.2) | 14.6 (12.5) | 14.3 (12.3) | |
| | 0.5 (**0.0**) | 13.2 (7.8) | 13.1 (7.4) | |
| [$COOH_s$]ttggcc | 14.3 (13.2) | 24.9 (21.9) | 24.3 (21.3) | |
| | 12.2 (13.0) | 23.3 (19.1) | 22.9 (18.5) | 10 (11) |
| $M^+$(Gln) | | | | B3LYP/MP2/CRENBL[e] |
| [COOH,CO]cgg$_+$g_t | 5.0 (5.0) | **0.0** (1.8) | **0.0** (0.3) | 6.8 (6.6)/3.2 (3.1) |
| | 6.5 (5.7) | **0.0** (0.1) | **0.0** (**0.0**) | 6.0 (2.2)/5.2 (5.3) |
| [N,CO,CO]tcggg | 8.8 (10.3) | 1.2 (4.5) | 0.9 (2.7) | 11.6 (10.3)/6.7 (5.4) |
| | 11.9 (12.3) | 2.0 (3.3) | 2.3 (3.5) | 8.7 (3.8)/1.0 (**0.0**) |
| [CO,CO]cgggt | 4.3 (3.7) | 0.9 (2.1) | 1.8 (1.5) | |
| | 5.7 (4.4) | 0.7 (0.3) | 0.9 (0.4) | |
| [COOH,CO]cgg_g$_+$t | 6.6 (3.4) | 1.4 (**0.0**) | 2.9 (**0.0**) | |
| | 13.9 (14.4)[f] | 1.0 (2.4)[f] | 3.0 (4.3)[f] | |
| [CO,CO]cgtgt | 1.5 ($0.0_s$) | 1.2 (1.6) | 5.4 (4.3) | |
| | 3.2 (0.5) | 1.7 (**0.0**) | 5.4 (3.5) | |
| [$CO_2^-$]ctggt | **0.0** (**0.0**) | 9.1 (10.9) | 6.0 (6.3) | **0.0** (**0.0**)/**0.0** (**0.0**) |
| | **0.0** (**0.0**) | 8.3 (9.3) | 3.3 (4.1) | **0.0** (**0.0**)/**0.0** (3.9) |
| [CO,CO]cgggg | 6.9 (5.9) | 6.2 (7.0) | 8.2 (7.5) | 9.5 (8.3)/3.5 (2.4) |
| | 8.7 (6.8) | 6.8 (5.8) | 7.8 (6.8) | 19.0 (15.3)/16.2 (16.3) |
| [$CO_2^-$]cgtgt | 0.4 (0.6) | 11.9 (13.9) | 9.8 (10.3) | |
| | 0.7 (0.2) | 10.7 (11.1) | 7.0 (7.3) | |

[a]Upper and lower values correspond to $Rb^+$ and $Cs^+$, respectively. Ground-state conformers in bold. [b]Relative free energies at 0 (298) K determined at the indicated level of theory with the def2-TZVPPD basis set using the associated B3LYP/def2-TZVPPD geometry. [c]B3LYP/CRENBL/6-31++G(d,p) results from ref 26. [d]B3P86/HW*/6-311+G(2d,2p)//B3LYP/6-311+G(d,p) values from ref 24. [e](B3LYP/MP2)/CRENBL/6-311++G(2d,2p)//B3LYP/6-31++G(d,p) free energies at 0 (298) K from ref 25. [f]Collapses to [CO,CO]cgggt at the B3LYP level. Values shown correspond to geometries calculated at the M06 level.

similar to N2 and N1, respectively, such that the shifts in thresholds are less than the computed excitation energies in all cases. Overall, our final BDEs are taken from the [N,CO,CO]/N1 analyses of the data.

**Experimental and Theoretical Results for $M^+$(Asn).** The present def2-TZVPPD results indicate that the $Rb^+$(Asn) complex has a [N,CO,CO] structure at both 0 and 298 K, with the [COOH,CO] conformer being low-lying and all other


dx.doi.org/10.1021/jp5001754 | J. Phys. Chem. B 2014, 118, 4300−4314

structures >11 kJ/mol higher in energy, Table S3. These results parallel those previously obtained using several different basis sets, with the only exception being B3P86 calculations (using any basis set),[24] as shown in Tables 3 and S3. For $Cs^+$(Asn), M06 retains the [N,CO,CO] ground state, but [COOH,CO] becomes the ground structure for B3LYP and MP2(full) calculations with [N,CO,CO] lying within 1 kJ/mol at both 0 and 298 K. Again this parallels previous calculations, with the B3P86 difference in energy being much greater than other levels of theory. In general, the present results stabilize the [N,CO,CO] conformer by 2−3 kJ/mol compared to the previous calculations, which used the HW*/6-311+G(2d,2p) basis set.

IRMPD spectra of $M^+$(Asn) are available for all five alkali metal cation complexes. The results are most consistent with [N,CO,CO] structures for all alkali metal cations. Contributions from [COOH,CO] cannot be ruled out for $Rb^+$(Asn) and $Cs^+$(Asn) but are not needed to explain the IRMPD spectra.[24] As for the present results, this conclusion is consistent with the calculations for $Rb^+$(Asn) (except for B3P86), which clearly establish [N,CO,CO] as the ground structure. In contrast, all levels of theory previously used identify [COOH,CO] as the ground structure of $Cs^+$(Asn) with [N,CO,CO] being very low-lying, consistent with the present results for B3LYP and MP2(full) calculations, Table 3. Interestingly, M06 finds that [N,CO,CO] is the ground-state structure for both $Rb^+$(Asn) and $Cs^+$(Asn), consistent with the IRMPD observations. Thus, the present theoretical results point to the M06 calculations as perhaps providing the best description of the relative energetics for $M^+$(Asn) complexes. Notably, the use of the large def2-TZVPPD basis set stabilizes the [N,CO,CO] conformer relative to the [COOH,CO] conformer, in agreement with the spectral results.

In the analysis of the TCID data, results were interpreted assuming the [N,CO,CO] ground state for $Rb^+$(Asn) and both [N,CO,CO] and [COOH,CO] conformers for $Cs^+$(Asn), Tables 1 and S1. The thresholds obtained for the latter differ by only 0.005 eV. We also checked whether dissociation to conformers of Asn other than the N1 ground state would influence the results. For all three excited conformers, the thresholds increase slightly, with N2 having the largest thresholds (1.46 and 1.22 eV for $Rb^+$ and $Cs^+$, respectively) and $\Delta S^{\dagger}_{1000}$ (44 and 41 J/mol K) values; however, the shifts in thresholds are less than the computed excitation energies in all but one case. For B3LYP calculations, N2 lies 2.3 kJ/mol above N1 and the threshold shift for $Rb^+$(Asn) is 2.8 kJ/mol, such that the difference in thresholds would be only 0.5 kJ/mol. Thus, our final bond energies can be taken from the [N,CO,CO]/N1 analyses of the TCID data.

**Experimental and Theoretical Results for $M^+$(Glu).** At the M06 and MP2(full) levels of theory, $Rb^+$(Glu) is predicted to have the [N,CO,CO]tggg$_+$g_t tridentate structure at both 0 and 298 K, with the [COOH,CO]cgggtt and [CO,CO]cgggtt structures being low-lying, within 4 kJ/mol, Table 3. For $Cs^+$(Glu), these three structures remain low in energy with [COOH,CO]cgggtt favored by MP2(full) at both 0 and 298 K, and M06 changing from [N,CO,CO]tggg$_+$g_t at 0 K to [CO,CO]cgggtt at 298 K. All three structures of $Cs^+$(Glu) lie within 2.3 kJ/mol of one another, with two alternate conformations [N,CO,CO]tggg_g$_+$t and [CO,CO]cgtgtt lying 3−8 kJ/mol above the ground state. In contrast, B3LYP results indicate that $Rb^+$(Glu) has the [CO,CO]cgtgtt structure at 0 and 298 K with two zwitterionic conformers, [$CO_2^-$]cgtgtt and [$CO_2^-$]ctggtt, as well as [CO,CO]cgggtt and [$COOH_s$]tgtgcc lying within ∼2 kJ/mol. For $Cs^+$(Glu), [$CO_2^-$]ctggtt and [$COOH_s$]tgtgcc are the 0 and 298 K ground structures, respectively. The B3LYP results in Table 3 are similar to the computations of O'Brien et al. at the B3LYP/CRENBL/6-31++G(d,p) level,[26] although the present calculations put the [N,CO,CO]tggg$_+$g_t conformer about 7 kJ/mol lower in relative energy and the [COOH,CO]ctccgt conformer about 5 kJ/mol higher. Notably, these authors identified only the [N,CO,CO]tggg$_+$g_t, [CO,CO]cgggtt, [COOH,CO]ctccgt, [$CO_2^-$]cgtgtt, and [$COOH_s$]ttggcc conformers, thereby missing several important low-energy structures, including the [COOH,CO]cgggtt structure, the MP2 ground state.

In their IRMPD spectra of $Cs^+$(Glu), O'Brien et al. find a spectrum similar to that of $Cs^+$(Asp) with major peaks at ∼1150, 1400, and 1750 $cm^{-1}$.[26] The spectrum is inconsistent with both zwitterionic [$CO_2^-$] (their calculated ground state) and [$COOH_s$] complexes and most closely resembled their calculated spectrum for [CO,CO]cgggtt. They concluded that this structure along with [N,CO,CO]tggg$_+$g_t and [COOH,CO]ctccgt were likely to contribute to the observed spectrum. The fact that the experimental spectrum is inconsistent with [$CO_2^-$] and [$COOH_s$] structures demonstrates that the present B3LYP calculations do not adequately represent the relative energies of the $Cs^+$(Glu) complexes. However, the M06 and MP2(full) calculations indicate that the [N,CO,CO]tggg$_+$g_t and [COOH,CO]cgggtt structures, where the latter was not located by O'Brien et al., are the ground state (the former for M06 at 0 K and the latter for MP2) or lie within 1.5 kJ/mol of the ground state, with [CO,CO]cgggtt being the ground state (M06 at 298 K) or lying within 2.3 kJ/mol of the ground state. Importantly, the calculated spectrum of this [COOH,CO]cgggtt structure shows intense bands at the same positions observed experimentally, Figure 4. This is in contrast with the [COOH,CO]ctccgt structure found by O'Brien et al.,[24] which has no strong band at 1150 $cm^{-1}$. Thus, we conclude with the same statement as O'Brien et al. that all three structures probably contribute to the observed spectrum, recognizing now that the [COOH,CO]cgggtt conformer is the form actually populated. Thus, the present M06 and MP2(full) calculations seem to predict the relative energies of these conformations well. Indeed, a superposition of the calculated spectra for these three structures reproduces the experimental spectrum reasonably well in terms of position, relative magnitudes, and shapes, Figure 4. (Such a superposition is in approximate agreement with an equilibrium distribution of these three conformers at 298 K calculated using the M06(MP2(full)) energetics: 32 (31)% [CO,CO]cgggtt, 27 (36)% [COOH,CO]cgggtt, 26 (21)% [N,CO,CO]tggggt, 14 (4)% [CO,CO]cgtgtt, and <1 (8)% all other conformers.)

In our analysis of the $M^+$(Glu) TCID data, variations associated with the different low-energy conformers of $M^+$(Glu) change the threshold energies by <0.02 eV for $Rb^+$ and by <0.003 eV for $Cs^+$, consistent with similar $\Delta S^{\dagger}_{1000}$ values, Table S1. For dissociation to conformers of Glu other than N1, the M06 and MP2 ground state, dissociation to N2 has a negligible effect on the threshold. For the B3LYP ground state, N3, the thresholds shift to higher energies by $0.03_1$ and $0.02_0$ eV for $Rb^+$(Glu) and $Cs^+$(Glu), respectively. Likewise, N4, which lies within 0.3 kJ/mol of the ground state at all three levels of theory, yields threshold energies lying $0.04_1$ and $0.02_6$ eV higher, respectively. In the latter two cases, the $\Delta S^{\dagger}_{1000}$


dx.doi.org/10.1021/jp5001754 | J. Phys. Chem. B 2014, 118, 4300−4314

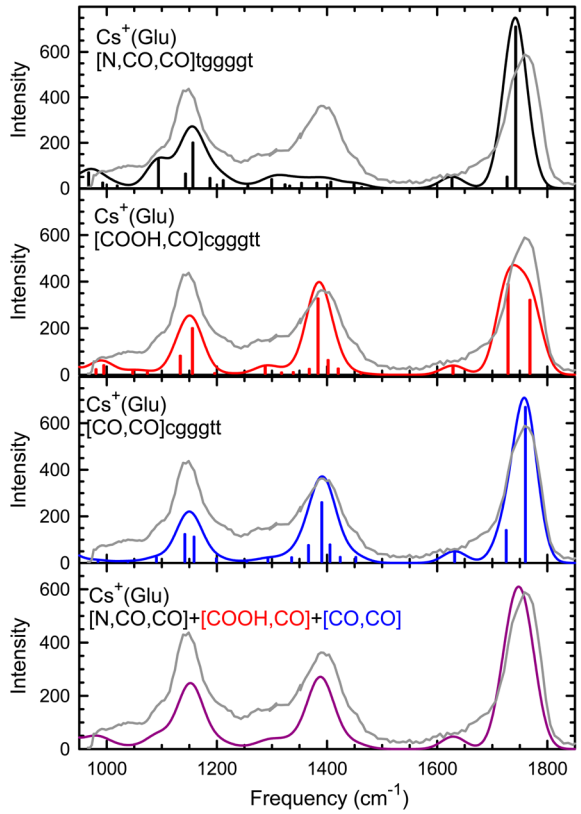


**Figure 4.** Comparison of the experimental IRMPD action spectrum for $Cs^+$(Glu)[26] (gray line, all panels) with IR spectra for three low-lying conformations predicted at the B3LYP/def2-TZVPPD level of theory and their average (bottom panel).

values increase substantially from 40 (N1) to 58 (N3) and 63 (N4) J/K·mol for $Rb^+$(Glu) and from 35 to 54 and 58 J/K·mol for $Cs^+$(Glu). Hence, dissociation will be dominated by the latter pathways (as demonstrated by an explicit examination of the rates of dissociation) and an average of these values is used as our best values, that is, our final bond energies are taken from the [N,CO,CO]/N3−N4 threshold energies.

**Experimental and Theoretical Results for $M^+$(Gln).** At the B3LYP level of theory, the zwitterionic [$CO_2^-$] complexes are the lowest energy structures at both 0 and 298 K, with the ctggt and cgtgt conformers lying within 1 kJ/mol of one another, Table 3. The B3LYP results in Table 3 are similar to the computations of Bush et al. at the B3LYP/CRENBL/6-311++G(2d,2p)//B3LYP/6-31++G(d,p) level.[25] Notably they elucidated only one member of each type of binding site and therefore did not consider alternative [CO,CO], [COOH,CO], [N,CO,CO], [COOH], [$CO_2^-$], and [$CO_2^-$,CO] conformers included in Tables 3 and S3. They also performed MP2/CRENBL/6-311++G(2d,2p)//B3LYP/6-31++G(d,p) calculations, Table 3, which again identify the zwitterion as the ground structure, in contrast to the present MP2 results. We identify several additional low-energy conformations, most notably the [CO,CO]cgggt geometry lying within 1 kJ/mol of the ground state, and the [COOH,CO]cgg$_+$g_t structure is now the ground state (or near ground state) at both 0 and 298 K. Notably, the previous MP2 calculations do find an increased stability of the [N,CO,CO] and [COOH,CO] structures compared to the B3LYP calculations.

Bush et al. measured the IRMPD spectra of $Li^+$(Gln), $Na^+$(Gln), $K^+$(Gln), and $Cs^+$(Gln), with the tridentate [N,CO,CO] conformer being the dominant contributor to the complexes of the three smaller metal cations, along with contributions from [CO,CO] and possibly [COOH,CO] for $Na^+$(Gln) and $K^+$(Gln).[25] For $Cs^+$(Gln), the latter structures probably dominate with smaller contributions from the [N,CO,CO] structure, the presence of which is confirmed by

**Table 4. Experimental and Theoretical Rubidium and Cesium Cation Bond Dissociation Energies to Asp, Glu, Asn, and Gln at 0 K (kJ/mol)**

| complex | expt[a] | B3LYP[b] | M06[b] | MP2(full)[b] |
|---|---|---|---|---|
| $Rb^+$(Asp) | 126.1 ± 6.8 | 119.9 (120.2) | 130.8 (131.0) | 126.8 (146.3) |
| $Cs^+$(Asp) | 108.9 ± 6.7 | 104.8 (105.0) | 120.4 (120.7) | 116.7 (129.0) |
| $Rb^+$(Glu) | 134.2 ± 7.7 | 121.9 (122.2) | 135.0 (135.0) | 131.1 (150.9) |
| | | 125.0 (125.1)[c] | | |
| $Cs^+$(Glu) | 112.6 ± 6.5 | 109.9 (110.0)[c] | 123.8 (124.2) | 120.6 (133.0) |
| | | 108.9 (109.1)[d] | 123.6 (124.1)[d] | 121.8 (134.2)[d] |
| | | 112.2 (112.4)[e] | | |
| $Rb^+$(Asn) | 138.4 ± 7.1 | 133.4 (133.8) | 143.6 (143.8) | 136.8 (157.2) |
| $Cs^+$(Asn) | 115.3 ± 6.9 | 117.8 (118.0) | 132.7 (133.4) | 126.2 (139.4) |
| | | 118.2 (118.6)[d] | 130.0 (130.5)[d] | 127.6 (140.1)[d] |
| $Rb^+$(Gln) | 144.2 ± 9.2 | 137.6 (137.8)[d] | 146.1 (146.3)[d] | 142.2 (162.7)[d] |
| | | 142.6 (142.8)[e] | | |
| $Cs^+$(Gln) | 128.1 ± 8.5 | 123.1 (123.3)[d] | 135.3 (135.7)[d] | 132.1 (145.4)[d] |
| | | 126.5 (126.6)[c] | | |
| | | 129.5 (129.8)[e] | | |
| MAD(Rb)[f] | | 6.7 (6.5) | 3.2 (3.3) | 1.9 (18.6) |
| MAD(Cs)[f] | | 2.7 (2.7) | 11.8 (12.3) | 8.0 (20.8) |
| MAD(all)[f] | | 4.7 (4.6) | 7.5 (7.8) | 4.9 (19.7) |

[a]Present experimental values from Tables 1 and S1 as detailed in the text. Uncertainties are one standard deviation. [b]Calculations performed at the stated level of theory using the def2-TZVPPD basis set on all atoms with geometries and vibrational frequencies calculated at the B3LYP/def2-TZVPPD level. All values counterpoise corrected with uncorrected values in parentheses. Values correspond to the [N,CO,CO] conformer, except as noted. [c][COOH,CO] conformer. [d][CO,CO] conformer. [e][$CO_2^-$] conformer. [f]Mean absolute deviation from the underlined or unique experimental values.


dx.doi.org/10.1021/jp5001754 | J. Phys. Chem. B 2014, 118, 4300−4314

characteristic bands at about 1100 and 1150 $cm^{-1}$. In agreement with the observed spectrum, the [COOH,CO] structure inverts the intensities of the two carbonyl stretch peaks compared with other structures, consistent with this species being a dominant contributor to the experimental spectrum (see Figure S3). This assignment agrees nicely with the present M06 and MP2 calculations, which place these three structures within 3.5 kJ/mol of the ground state, either [COOH,CO]cgg$_+$g_t, [COOH,CO]cgg_g$_+$t, or [CO,CO]cgtgt. Calculated spectra for the two [COOH,CO] and two [CO,CO] structures are similar, although [CO,CO]cgtgt is broader and less intense at the band near 1380 $cm^{-1}$. A superposition of the calculated spectra for [COOH,CO]-cgg$_+$g_t, [CO,CO]cgtgt, and [N,CO,CO]tcggg reproduces the experimental spectrum with reasonable accuracy, Figure S3. (Such a superposition is in approximate agreement with an equilibrium distribution of these three conformers at 298 K calculated using the M06(MP2(full)) energetics: 27 (35)% [COOH,CO]cgg$_+$g_t, 28 (9)% [CO,CO]cgtgt, 24 (30)% [CO,CO]cgggt, 7 (9)% [N,CO,CO]tcggg, 10 (6)% [COOH,CO]cgg_g$_+$t, and <4 (11)% all other conformers.) None of the experimental spectra, including that for $Cs^+$(Gln), are consistent with zwitterionic [$CO_2^-$] or [$COOH_s$] structures, which demonstrates that B3LYP calculations do not accurately represent the $Cs^+$(Gln) relative energies.

Analyses of the $M^+$(Gln) TCID data show variations in the threshold energies as different conformers of $M^+$(Gln) are assumed, with changes of <0.06 eV for $Rb^+$ and <0.03 eV for $Cs^+$, consistent with similar $\Delta S^{\dagger}_{1000}$ values. For dissociation to conformers of Gln other than N1 (the B3LYP ground state), dissociation to N3 (the M06 and MP2 ground state) has a larger kinetic shift by 0.05 − 0.07 eV with a $\Delta S^{\dagger}_{1000}$ value lower by 18 J/(mol K). Dissociation to N2 behaves similarly to N1, and that to N4 is comparable to dissociation to N3. In this system, the dissociation kinetics should be dominated by the channel with the largest $\Delta S^{\dagger}_{1000}$ value and the lowest energy, N1. On the basis of the IRMPD results, our final bond energies for both $Rb^+$(Gln) and $Cs^+$(Gln) are taken as an average of the [COOH,CO]/N1 (two structures), [CO,CO]/N1 (two structures), and [N,CO,CO]/N1 analyses of the data. The use of this average leads to slightly larger experimental uncertainties in the final bond energies than those determined for the other systems.

## DISCUSSION

Our final experimental BDEs for the eight complexes investigated here are provided in Table 4. We also convert these 0 K BDEs to 298 K bond enthalpies and free energies of dissociation, as listed in Table S6 of the Supporting Information. Notably, these conversions depend on the specific conformers involved, so multiple values are provided.

**Comparison of Theoretical and Experimental Bond Dissociation Energies.** Table 4 compares the experimental and theoretical BDEs for the $Rb^+$(AA) and $Cs^+$(AA) complexes, where AA = Asp, Glu, Asn, and Gln. For M06 and MP2(full) values, the BDEs of the most stable conformers are shown in all cases, whereas in the case of the B3LYP values, the most stable conformers include zwitterionic structures (Glu and Gln), which IRMPD results demonstrate are not present. Thus, B3LYP results used for comparison correspond to the most strongly bound species that has a confirmed population. For rubidium and cesium, experiments indicate that the relative BDEs increase in the order Asp < Glu < Asn < Gln, in agreement with theory. The predicted range between the Asp and Gln experimental BDEs is 18 kJ/mol for $Rb^+$, compared to theoretical ranges at the B3LYP, M06, and MP2(full) levels of 18, 15, and 15 kJ/mol, respectively. For $Cs^+$, the experimental range is 19 kJ/mol compared to 22, 15, and 15 kJ/mol, respectively. M06 results are systematically high compared to experiment, whereas B3LYP is systematically lower than experiment except for $Cs^+$(Asn), which is only 2.5 kJ/mol above experiment. (This trend remains true even if the more strongly bound zwitterionic species are considered, except that the computed BDE for $Cs^+$(Gln) [$CO_2^-$] is 1.4 kJ/mol above experiment.) MP2(full) yields results both above and below experiment with values for $Rb^+$ complexes being slightly low and those for $Cs^+$ complexes being high. These trends for the MP2(full) values are shown in Figure 5, with comparable results for the B3LYP and M06 levels of theory shown in Figure S4 of the Supporting Information. The lowest overall mean absolute deviation (MAD) between experiment and theory is similar for B3LYP and MP2(full) calculations at about 5 kJ/mol, whereas that for M06 is 7.5 kJ/mol. These deviations are comparable to the experimental uncertainties. MADs for theoretical values without counterpoise corrections are virtually the same as those with counterpoise for the two DFT approaches, whereas the counterpoise corrections are clearly needed for the MP2(full) approach as the MAD without them increases to 20 kJ/mol, with all theoretical values being systematically high.

It is worth noting that MP2(full) calculations reproduce the $Rb^+$ values particularly well (MAD = 2 kJ/mol), whereas B3LYP reproduces the $Cs^+$ values better (MAD = 3 kJ/mol) than the other two approaches. These results parallel those obtained in our previous studies of other $Rb^+$(AA) and $Cs^+$(AA) BDEs, where AA = Gly, Pro, Ser, Thr, Cys, Met, Phe, Tyr, Trp, and His.[13,14,17,19,20] For these 10 amino acids, the MADs for the $Rb^+$ complexes are 5 ± 3, 6 ± 3, and 4 ± 3 kJ/mol at the B3LYP, M06, and MP2(full) levels, respectively, and 5 ± 4, 8 ± 4, and 8 ± 4 kJ/mol, respectively, for the $Cs^+$ complexes. Overall, for both metal cations and all 14 amino acids, the MADs are 5 ± 3, 7 ± 4, and 6 ± 4 kJ/mol, respectively.

Figure 5 illustrates the overall agreement between experiment and the MP2(full)/def2-TZVPPD results for the present

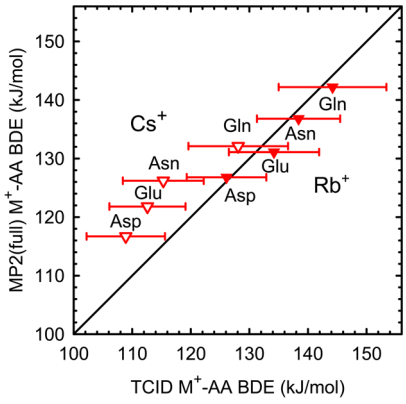


**Figure 5.** Experimental 0 K bond dissociation energies (in kJ/mol) for $M^+$(Asp), $M^+$(Glu), $M^+$(Asn), and $M^+$(Gln) for $M^+$ = $Rb^+$ (solid symbols) and $Cs^+$ (open symbols) plotted vs MP2(full)/def2-TZVPPD//B3LYP/def2-TZVPPD theoretical values for the calculated ground-state species. The diagonal line shows perfect agreement.


dx.doi.org/10.1021/jp5001754 | J. Phys. Chem. B 2014, 118, 4300−4314

systems. It can be seen that these results are nearly within experimental error for most values and the same is true for B3LYP results, Figure S4. The M06 level of theory is similar to the MP2(full) results except being systematically higher by 4.3 ± 1.6 kJ/mol. All levels of theory correctly predict the relative values among these four amino acids for a particular metal cation.

**Trends in Bond Energies: Metal Cation Identity and Side-Chain Substituent Effects.** The functional groups of amino acids solvate the charge of metal cations by electrostatic forces, including ion induced-dipole, ion-quadrupole, and ion-dipole forces. Experimental results for the $M^+$(AA) BDEs, where $M^+$ = $Rb^+$ and $Cs^+$ and AA = Asp, Glu, Asn, and Gln (Table 4), are smaller than the values for the analogous complexes with $M^+$ = $Na^+$ and $K^+$,[22,23] as shown in Figure 6, as is also true for all other AAs.[13,14,17−21] Because the radii of the metal cations increases from $Na^+$ to $Cs^+$ (0.98, 1.33, 1.49, and 1.69 Å, respectively[80]), the bond distances necessarily increase leading to reduced electrostatic interactions, approximately linearly as the inverse of the ionic radius. (Note that such a dependence could imply a long-range Coulombic potential; however, the true interactions must be combinations of ion-dipole ($r^{-2}$), ion-quadrupole ($r^{-3}$), and ion-induced dipole ($r^{-4}$) forces along with complex chelation effects that alter these long-range forces at the shorter bond distances associated with these complexes. Accordingly, plots of the BDEs versus $r^{-2}$ and $r^{-4}$ are no longer linear.) The lines shown in Figure 6 are linear regression fits (constrained to pass through the origin) for the Gly, Asp, and Gln data. Similar fits to the Glu and Asn data lie in between those for Asp and Gln. Slopes for the Gly, Asp, Glu, Asn, and Gln complexes are 158 ± 6, 191 ± 8, 197 ± 8, 204 ± 7, and 212 ± 6 Å kJ/mol, respectively. The trends are nicely systematic in that the $K^+$(AA), $Rb^+$(AA), and $Cs^+$(AA) BDEs for these four amino acids are 76 ± 1%, 66 ± 2%, and 57 ± 2% of the $Na^+$(AA) BDEs, with average differences of 50 ± 3 kJ/mol between $Na^+$(AA) and $K^+$(AA), 19 ± 2 kJ/mol between $K^+$(AA) and $Rb^+$(AA), and 20 ± 3 kJ/mol between $Rb^+$(AA) and $Cs^+$(AA).

**Trends in Bond Energies: Effects of Polarizability and Polar Side Chains on $Rb^+$(AA) and $Cs^+$(AA).** Figure 6 also illustrates the effect of the side chain on the $M^+$(AA) BDEs studied here. Clearly, the longer side chains of Glu and Gln bind more strongly than the shorter side chains of Asp and Asn, respectively, an effect that is largely attributable to the increased polarizability of the longer side chain. The present experimental studies determine that the longer chain length of Glx compared to Asx increases the $Rb^+$ and $Cs^+$ binding affinities by 8 ± 4 kJ/mol, comparable to the predictions of theory: 5 ± 3 (B3LYP), 3 ± 1 (M06), and 5 ± 1 (MP2) kJ/mol. These increases are somewhat greater than those observed for the comparable complexes of $Na^+$ and $K^+$, where systematic increases of 4 ± 1 and 5 ± 1 kJ/mol were observed.[22,23] It is also apparent from Figure 6 that the amide side chains of Asn and Gln bind more tightly than the acidic acid side chains of Asp and Glu for all four metal cations. Previously, the increases for the $Na^+$ and $K^+$ complexes were measured as 14 ± 1 and 9 ± 1 kJ/mol, respectively,[22,23] whereas here $Rb^+$ and $Cs^+$ bind to the amides more strongly than the acids by 11 ± 2 and 11 ± 6 kJ/mol, respectively. Clearly, the effect is nearly the same for all four metal cations. Previously, this has been explained by an inductive effect of the hydroxyl group of the carboxylic acid side chain, which removes electron density from the carbonyl binding site compared to the amide group of the carboxamide side chain.[22,23]

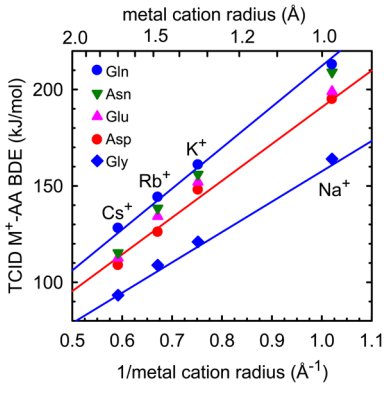


**Figure 6.** Experimental 0 K bond dissociation energies (in kJ/mol) for $M^+$(Gly) (blue diamonds), $M^+$(Asp) (red circles), $M^+$(Glu) (magenta triangles), $M^+$(Asn) (green inverted triangles), and $M^+$(Gln) (blue circles) for $M^+$ = $Na^+$, $K^+$, $Rb^+$, and $Cs^+$ are plotted vs the inverse metal cation radius (in $Å^{-1}$). The lines are linear regression fits to the $M^+$(Gly), $M^+$(Asp), and $M^+$(Gln) data constrained to pass through the origin.

As noted above, we have previously found a correlation between the polarizabilities of the amino acids Gly, Met, Phe, Tyr, and Trp and their BDEs to $Na^+$ and $K^+$.[9,21] This correlation then allows a more accurate assessment of the enhanced binding derived from more polar side chains for these two metal cations.[16,20,22,23] For $Na^+$ and $K^+$, it was found that Ser, Thr, Asp, Asn, Glu, Gln, and His all showed enhanced binding compared to values predicted from the polarizability correlation. BDEs to Ser, Thr, Asn, Gln, and His form series that parallel those for the aliphatic amino acids. For these amino acids, the average enhancement is approximately 28 and 24 kJ/mol for $Na^+$ and $K^+$, respectively.[18,20] Asp and Glu form a separate series in between the polar and aliphatic series (enhancements of about 15 kJ/mol for both $Na^+$ and $K^+$), consistent with the reduced binding resulting from the inductive effect of the hydroxyl group.

We recently established this same correlation for both $Rb^+$ and $Cs^+$ with these amino acids, as shown in Figure 7.[19] Using this as a baseline for the influence of polarizability on the BDEs, the influence of polar side chains can now be quantitatively examined. (All isotropic molecular polarizabilities used here were calculated at the PBE0/6-311+G(2d,2p) level of theory using the B3LYP/6-311G(d,p) optimized geometries of the neutral amino acid in the metal cationized complexes. This level of theory has been shown to provide polarizabilities that are in good agreement with measured values.[81]) Figure 7 shows that the polar side chains of Ser, Thr, Asp, Asn, Glu, Gln, and His also lead to enhanced binding to $Rb^+$ and $Cs^+$, although the different side chains behave somewhat differently compared to the lighter metal cations. For $Rb^+$, Ser and Thr show an enhancement of only 5−7 kJ/mol,[13,14] with Asp, Glu, and His showing an average enhancement of ∼15 kJ/mol,[20] and Asn and Gln are higher than the polarizability trend by ∼24 kJ/mol. For $Cs^+$, Ser and Thr lie ∼7 kJ/mol above the trend line,[13,14] with Asp, Glu, and His forming a consistent series lying 10 kJ/mol above the polarizability trend,[20] and Asn and Gln are higher still, by 15 and 24 kJ/mol, respectively. Thus, the enhancement for the shortest polar side chains (only two atoms long) of Ser and Thr change as a function of the metal, dropping from 28 to 24 to 10 to 7 kJ/mol in going from $Na^+$ to


dx.doi.org/10.1021/jp5001754 | J. Phys. Chem. B 2014, 118, 4300−4314

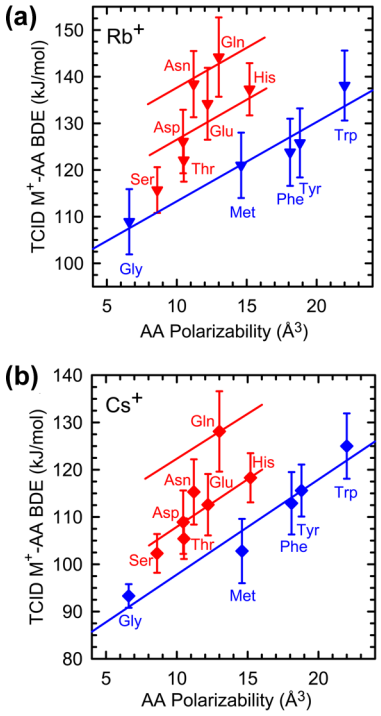


**Figure 7.** Experimental 0 K bond dissociation energies (in kJ/mol) for $M^+$(Gly), $M^+$(Met), $M^+$(Phe), $M^+$(Tyr), and $M^+$(Trp) (in blue) and $M^+$(Ser), $M^+$(Thr), $M^+$(Asp), $M^+$(Asn), $M^+$(Glu), $M^+$(Gln), and $M^+$(His) (in red) for $M^+$ = $Rb^+$ (a) and $Cs^+$ (b) are plotted vs the calculated polarizability volume of the amino acid (in Å$^3$). Lines (blue) through the aliphatic amino acids are linear regression fits to the data for each metal cation. Lines (red) through the polar amino acids have the same slope but are displaced upward by 13 and 24 ($Rb^+$) and 8 and 22 ($Cs^+$) kJ/mol.

$K^+$ to $Rb^+$ to $Cs^+$. Such a decrease is presumably a consequence of both the larger metal cation radius and the fact that the larger cations cannot take advantage of binding in a tridentate conformation as well as the smaller cations, as previously demonstrated elsewhere.[13,14] In contrast, for Gln with a side chain length of four atoms, the enhancement is largely independent of the metal, being 24 − 28 kJ/mol for all four metal cations, suggesting that the longer side chain allows better tridentate binding for the strongly binding carbonyl group of the carboxamide. For Asp, Glu, and His, with three, four, and three atom side chain lengths, the enhancements drop from 28 ($Na^+$) to 24 ($K^+$) to 15 ($Rb^+$) and 15 ($Cs^+$) kJ/mol, again consistent with better tridentate binding than the short side chain AAs. However, binding is less effective than with Gln because the side chain moieties of Asp, Glu, and His do not bind as tightly as the carboxamide. Asn, with the same but shorter side chain group than Gln, shows a trend of 28 ($Na^+$), 24 ($K^+$), 24 ($Rb^+$), and 15 ($Cs^+$) kJ/mol, intermediate between the strong effect of Gln and the weaker effects of Asp, Glu, and His.

## CONCLUSIONS

The kinetic energy dependences of the collision-induced dissociation of $Rb^+$(AA) and $Cs^+$(AA), where AA = Asp, Glu, Asn, and Gln, with Xe are examined in a guided ion beam tandem mass spectrometer. Loss of the intact amino acid from the complex is the only dissociation pathway observed in all eight systems. Detailed modeling of the experimental cross sections yields BDEs for $Rb^+$−AA and $Cs^+$−AA at 0 K and values at 298 K are calculated using the computed molecular parameters for the ground-state conformations. The energy thresholds for binding to the amino acids follow the order of $M^+$(Asp) < $M^+$(Glu) < $M^+$(Asn) < $M^+$(Gln), in agreement with quantum chemical calculations. When the def2-TZVPPD basis set is used, B3LYP, M06, and MP2(full) approaches including zero point energy corrections and counterpoise corrections for basis set superposition errors generally agree well with our experimental values, Table 4. M06 values tend to be high, with MP2 providing particularly good agreement for the $Rb^+$(AA) complexes and B3LYP for the $Cs^+$(AA) complexes, similar to previous work.[19]

As expected, the binding energies for these four amino acids to $Na^+$, $K^+$, $Rb^+$, and $Cs^+$ decrease as the metal cation increases in size, Figure 6. When compared with previous work that establishes a baseline correlation between $M^+$−AA BDEs and the polarizability of the amino acid,[19] the present work demonstrates that the carboxylic acid and carboxamide side chains enhance the binding, as previously found for the smaller alkali metal cations.[22,23] The average enhancement for Gln is found to be fairly uniform for all four alkali metal cations, whereas Asp, Glu, and Asn exhibit a modest decline as the metal cation gets larger. This is attributed to differences associated with the side chain length along with the difficulty that the larger rubidium and cesium cations cannot take full advantage of binding in a tridentate conformation, as demonstrated previously.[13,14] Overall, the trends elucidated in these studies provide a powerful means of ascertaining the effects of individual side chain functional groups on their binding affinities to metal cations, which should prove useful in quantitatively assessing alkali metal cation−protein interactions as well as those that occur in even more complex biological systems.

## ASSOCIATED CONTENT

### Supporting Information

Table of TCID data analyses for all conformations of $M^+$(AA) reactants and AA products considered. Tables of theoretical geometries and relative energies for rubidium and cesium-cation bound to Asp, Asn, Glu, and Gln. Tables of 298 K enthalpies and free energies of dissociation for various complex conformations. Tables comparing relative energies for geometries calculated at the B3LYP and M06 levels of theory. Figures of experimental results and data analysis for all eight metal cation-amino acid systems. Figures comparing IRMPD spectra for $Cs^+$(Asp) and $Cs^+$(Gln) with present calculations. This material is available free of charge via the Internet at http://pubs.acs.org.

## AUTHOR INFORMATION

### Notes

The authors declare no competing financial interest.

## ACKNOWLEDGMENTS

This work is supported by the National Science Foundation, CHE-0911191 (M.T.R.) and CHE-1049580 (P.B.A.). A grant of computer time from the Center for High Performance Computing at the University of Utah is gratefully acknowledged. Thanks to E. R. Williams, J. T. O'Brien, and J. Oomens for making their IRMPD spectra available.

## REFERENCES


(1) Hood, S. L.; Comar, C. L. Metabolism of Cesium-137 in Rats and Farm Animals. *Arch. Biochem. Biophys.* **1953**, *45*, 423−433.
(2) Beauge, L. A.; Sjodin, R. A. Transport of Caesium in Frog Muscle. *J. Physiol.* **1968**, *194*, 105−123.
(3) Matsuda, H.; Matsuura, H.; Noma, A. Triple-Barrel Structure of Inwardly Rectifying $K^+$ Channels Revealed by $Cs^+$ and $Rb^+$ Block in Guinea-Pig Heart Cells. *J. Physiol.* **1989**, *413*, 139−157.
(4) Spruce, A. E.; Standen, N. B.; Stanfield, P. R. Rubidium Ions and the Gating of Delayed Rectifier Potassium Channels of Frog Skeletal Muscle. *J. Physiol.* **1989**, *411*, 597−610.
(5) Relman, S. R.; Lambie, A. T.; Burrows, B. A.; Roy, A. M. Cation Accumulation by Muscle Tissue: The Displacement of Potassium by Rubidium and Cesium in the Living Animal. *J. Clin. Invest.* **1957**, *36*, 1249−1256.
(6) Richmond, C. R. Retention and Excretion of Radionuclides of the Alkali Metals by Five Mammalian Species. *Health Phys.* **1980**, *38*, 1111−1153.
(7) Yen, C. K.; Budinger, T. F. Evaluation of Blood−Brain Barrier Permeability Changes in Rhesus Monkeys and Man Using $^{82}Rb$ and Positron Emission Tomography. *J. Comp. Assist. Tomog.* **1981**, *5*, 792−799.
(8) Gal, J.-F.; Maria, P.-C.; Massi, L.; Mayeux, C.; Burk, P.; Tammiku-Taul, J. Cesium Cation Affinities and Basicities. *Int. J. Mass Spectrom.* **2007**, *267*, 7−23.
(9) Rodgers, M. T.; Armentrout, P. B. A Thermodynamic "Vocabulary" for Metal Ion Interactions in Biological Systems. *Acc. Chem. Res.* **2004**, *37*, 989−998.
(10) Moision, R. M.; Armentrout, P. B. An Experimental and Theoretical Dissection of Sodium Cation/Glycine Interactions. *J. Phys. Chem. A* **2002**, *106*, 10350−10362.
(11) Moision, R. M.; Armentrout, P. B. An Experimental and Theoretical Dissection of Potassium Cation/Glycine Interactions. *Phys. Chem. Chem. Phys.* **2004**, *6*, 2588−2599.
(12) Rodgers, M. T.; Armentrout, P. B. A Critical Evaluation of the Experimental and Theoretical Determination of Lithium Cation Affinities. *Int. J. Mass Spectrom.* **2007**, *267*, 167−182.
(13) Bowman, V. N.; Heaton, A. L.; Armentrout, P. B. Metal Cation Dependence of Interactions with Amino Acids: Bond Energies of $Rb^+$ to Gly, Ser, Thr, and Pro. *J. Phys. Chem. B* **2010**, *114*, 4107−4114.
(14) Armentrout, P. B.; Chen, Y.; Rodgers, M. T. Metal Cation Dependence of Interactions with Amino Acids: Bond Energies of $Cs^+$ to Gly, Pro, Ser, Thr, and Cys. *J. Phys. Chem. A* **2012**, *116*, 3989−3999.
(15) Moision, R. M.; Armentrout, P. B. The Special Five-Membered Ring of Proline: An Experimental and Theoretical Investigation of Alkali Metal Cation Interactions with Proline and Its Four- and Six-Membered Ring Analogues. *J. Phys. Chem. A* **2006**, *110*, 3933−3946.
(16) Ye, S. J.; Clark, A. A.; Armentrout, P. B. An Experimental and Theoretical Investigation of Alkali Metal Cation Interactions with Hydroxyl Side Chain Amino Acids. *J. Phys. Chem. B* **2008**, *112*, 10291−10302.
(17) Armentrout, P. B.; Armentrout, E. I.; Clark, A. A.; Cooper, T. E.; Stennett, E. M. S.; Carl, D. R. An Experimental and Theoretical Study of Alkali Metal Cation Interactions with Cysteine. *J. Phys. Chem. B* **2010**, *114*, 3927−3937.
(18) Armentrout, P. B.; Gabriel, A.; Moision, R. M. An Experimental and Theoretical Study of Alkali Metal Cation/Methionine Interactions. *Int. J. Mass Spectrom.* **2009**, *283*, 56−68.
(19) Armentrout, P. B.; Yang, B.; Rodgers, M. T. Metal Cation Dependence of Interactions with Amino Acids: Bond Energies of $Rb^+$ and $Cs^+$ to Met, Phe, Tyr, and Trp. *J. Phys. Chem. A* **2013**, *117*, 3771−3781.
(20) Armentrout, P. B.; Citir, M.; Chen, Y.; Rodgers, M. T. Thermochemistry of Alkali Metal Cation Interactions with Histidine: Influence of the Side Chain. *J. Phys. Chem. A* **2012**, *116*, 11823−11832.
(21) Ruan, C.; Rodgers, M. T. Cation-$\pi$ Interactions: Structures and Energetics of Complexation of $Na^+$ and $K^+$ with the Aromatic Amino Acids, Phenylalanine, Tyrosine and Tryptophan. *J. Am. Chem. Soc.* **2004**, *126*, 14600−14610.
(22) Heaton, A. L.; Moision, R. M.; Armentrout, P. B. Experimental and Theoretical Studies of Sodium Cation Interactions with the Acidic Amino Acids and Their Amide Derivatives. *J. Phys. Chem. A* **2008**, *112*, 3319−3327.
(23) Heaton, A. L.; Armentrout, P. B. Experimental and Theoretical Studies of Potassium Cation Interactions with the Acidic Amino Acids and Their Amide Derivatives. *J. Phys. Chem. B* **2008**, *112*, 12056−12065.
(24) Heaton, A. L.; Bowman, V. N.; Oomens, J.; Steill, J. D.; Armentrout, P. B. Infrared Multiple Photon Dissociation Spectroscopy of Cationized Asparagine: Effects of Alkali-Metal Cation Size on Gas-Phase Conformation. *J. Phys. Chem. A* **2009**, *113*, 5519−5530.
(25) Bush, M. F.; Oomens, J.; Saykally, R. J.; Williams, E. R. Alkali Metal Ion Binding to Glutamine and Glutamine Derivatives Investigated by Infrared Action Spectroscopy and Theory. *J. Phys. Chem. A* **2008**, *112*, 8578−8584.
(26) O'Brien, J. T.; Prell, J. S.; Steill, J. D.; Oomens, J.; Williams, E. R. Interactions of Mono- and Divalent Metal Ions with Aspartic and Glutamic Acid Investigated with IR Photodissociation Spectroscopy and Theory. *J. Phys. Chem. A* **2008**, *112*, 10823−10830.
(27) Armentrout, P. B.; Rodgers, M. T.; Oomens, J.; Steill, J. D. Infrared Multiphoton Dissociation Spectroscopy of Cationized Serine: Effects of Alkali-Metal Cation Size on Gas-Phase Conformation. *J. Phys. Chem. A* **2008**, *112*, 2248−2257.
(28) Rodgers, M. T.; Armentrout, P. B.; Oomens, J.; Steill, J. D. Infrared Multiphoton Dissociation Spectroscopy of Cationized Threonine: Effects of Alkali-Metal Cation Size on Gas-Phase Conformation. *J. Phys. Chem. A* **2008**, *112*, 2258−2267.
(29) Citir, M.; Stennett, E. M. S.; Oomens, J.; Steill, J. D.; Rodgers, M. T.; Armentrout, P. B. Infrared Multiple Photon Dissociation Spectroscopy of Cationized Cysteine: Effects of Metal Cation Size on Gas-Phase Conformation. *Int. J. Mass Spectrom.* **2010**, *297*, 9−17.
(30) Carl, D. R.; Cooper, T. E.; Oomens, J.; Steill, J. D.; Armentrout, P. B. Infrared Multiple Photon Dissociation Spectroscopy of Cationized Methionine: Effects of Alkali-Metal Cation Size on Gas-Phase Conformation. *Phys. Chem. Chem. Phys.* **2010**, *12*, 3384−3398.
(31) Forbes, M. W.; Bush, M. F.; Polfer, N. C.; Oomens, J.; Dunbar, R. C.; Williams, E. R.; Jockusch, R. A. Infrared Spectroscopy of Arginine Cation Complexes: Direct Observation of Gas-Phase Zwitterions. *J. Phys. Chem. A* **2007**, *111*, 11759−11770.
(32) Polfer, N. C.; Oomens, J.; Dunbar, R. C. IRMPD Spectroscopy of Metal-Ion/Tryptophan Complexes. *Phys. Chem. Chem. Phys.* **2006**, *8*, 2744−2751.
(33) Dunbar, R. C.; Steill, J. D.; Oomens, J. Cationized Phenylalanine Conformations Characterized by IRMPD and Computation for Singly and Doubly Charged Ions. *Phys. Chem. Chem. Phys.* **2010**, *12*, 13383−13393.
(34) Citir, M.; Hinton, C. S.; Oomens, J.; Steill, J. D.; Armentrout, P. B. Infrared Multiple Photon Dissociation Spectroscopy of Cationized Histidine: Effects of Metal Cation Size on Gas-Phase Conformation. *J. Phys. Chem. A* **2012**, *116*, 1532−1541.
(35) Rodgers, M. T. Substituent Effects in the Binding of Alkali Metal Ions to Pyridines Studied by Threshold Collision-Induced Dissociation and Ab Initio Theory: The Methylpyridines. *J. Phys. Chem. A* **2001**, *105*, 2374−2383.
(36) Moision, R. M.; Armentrout, P. B. An Electrospray Source for Thermochemical Investigation with the Guided Ion Beam Mass Spectrometer. *J. Am. Soc. Mass Spectrom.* **2007**, *18*, 1124−1134.
(37) Ye, S. J.; Armentrout, P. B. Absolute Thermodynamic Measurements of Alkali Metal Cation Interactions with a Simple Dipeptide and Tripeptide. *J. Phys. Chem. A* **2008**, *112*, 3587−3596.
(38) Carl, D. R.; Moision, R. M.; Armentrout, P. B. Binding Energies for the Inner Hydration Shells of $Ca^{2+}$: An Experimental and Theoretical Investigation of $Ca^{2+}(H_2O)_x$ Complexes ($x$ = 5−9). *Int. J. Mass Spectrom.* **2007**, *265*, 308−325.
(39) Chen, Y.; Rodgers, M. T. Structural and Energetic Effects in the Molecular Recognition of Protonated Peptidomimetic Bases by 18-Crown-6. *J. Am. Chem. Soc.* **2012**, *134*, 2313−2324.

(40) Chen, Y.; Rodgers, M. T. Structural and Energetic Effects in the Molecular Recognition of Amino Acids by 18-Crown-6. *J. Am. Chem. Soc.* **2012**, *134*, 5863−5875.
(41) Aristov, N.; Armentrout, P. B. Collision-Induced Dissociation of Vanadium Monoxide Ion. *J. Phys. Chem.* **1986**, *90*, 5135−5140.
(42) Dalleska, N. F.; Honma, K.; Sunderlin, L. S.; Armentrout, P. B. Solvation of Transition Metal Ions by Water. Sequential Binding Energies of $M^+(H_2O)_x$ ($x$ = 1−4) for M = Ti−Cu Determined by Collision-Induced Dissociation. *J. Am. Chem. Soc.* **1994**, *116*, 3519−3528.
(43) Daly, N. R. Scintillation Type Mass Spectrometer Ion Detector. *Rev. Sci. Instrum.* **1960**, *31*, 264−267.
(44) Ervin, K. M.; Armentrout, P. B. Translational Energy Dependence of $Ar^+ + XY \rightarrow ArX^+ + Y$ (XY = $H_2$, $D_2$, HD) from Thermal to 30 eV cm. *J. Chem. Phys.* **1985**, *83*, 166−189.
(45) Loh, S. K.; Hales, D. A.; Lian, L.; Armentrout, P. B. Collision-Induced Dissociation of $Fe_n^+$ ($n$ = 2−10) with Xe: Ionic and Neutral Iron Cluster Binding Energies. *J. Chem. Phys.* **1989**, *90*, 5466−5485.
(46) Khan, F. A.; Clemmer, D. E.; Schultz, R. H.; Armentrout, P. B. Sequential Bond Energies of $Cr(CO)_x^+$, $x$ = 1−6. *J. Phys. Chem.* **1993**, *97*, 7978−7987.
(47) Rodgers, M. T.; Ervin, K. M.; Armentrout, P. B. Statistical Modeling of Collision-Induced Dissociation Thresholds. *J. Chem. Phys.* **1997**, *106*, 4499−4508.
(48) Armentrout, P. B.; Ervin, K. M.; Rodgers, M. T. Statistical Rate Theory and Kinetic Energy-Resolved Ion Chemistry—Theory and Applications. *J. Phys. Chem. A* **2008**, *112*, 10071−10085.
(49) Muntean, F.; Armentrout, P. B. Guided Ion Beam Study of Collision-Induced Dissociation Dynamics: Integral and Differental Cross Sections. *J. Chem. Phys.* **2001**, *115*, 1213−1228.
(50) Beyer, T. S.; Swinehart, D. F. Number of Multiply-Restricted Partitions. *Commun. ACM* **1973**, *16*, 379.
(51) Stein, S. E.; Rabinovitch, B. S. Accurate Evaluation of Internal Energy Level Sums and Densities Including Anharmonic Oscillators and Hindered Rotors. *J. Chem. Phys.* **1973**, *58*, 2438−2445.
(52) Stein, S. E.; Rabinovich, B. S. On the Use of Exact State Counting Methods in RRKM Rate Calculations. *Chem. Phys. Lett.* **1977**, *49*, 183−188.
(53) Gilbert, R. G.; Smith, S. C. *Theory of Unimolecular and Recombination Reactions*; Blackwell Scientific: London, 1990.
(54) Robinson, P. J.; Holbrook, K. A. *Unimolecular Reactions*; Wiley Interscience: New York, 1972.
(55) Rodgers, M. T.; Armentrout, P. B. Statistical Modeling of Competitive Threshold Collision-Induced Dissociation. *J. Chem. Phys.* **1998**, *109*, 1787−1800.
(56) More, M. B.; Ray, D.; Armentrout, P. B. Intrinsic Affinities of Alkali Cations for 15-Crown-5 and 18-Crown-6: Bond Dissociation Energies of Gas-Phase $M^+$-Crown Ether Complexes. *J. Am. Chem. Soc.* **1999**, *121*, 417−423.
(57) More, M. B.; Ray, D.; Armentrout, P. B. Cation-Ether Complexes in the Gas Phase: Bond Dissociation Energies of $M^+$(dimethyl ether)$_x$, $x$ = 1−3, $M^+$(1,2-dimethoxyethane)$_x$, $x$ = 1 and 2, and $M^+$(12-crown-4), where M = Rb and Cs. *J. Phys. Chem. A* **1997**, *101*, 7007−7017.
(58) Armentrout, P. B.; Austin, C. A.; Rodgers, M. T. Alkali Metal Cation Interactions with 12-Crown-4 in the Gas Phase: Revisited. *Int. J. Mass Spectrom.* **2012**, *330*−*332*, 16−26.
(59) Chantry, P. J. Doppler Broadening in Beam Experiments. *J. Chem. Phys.* **1971**, *55*, 2746−2759.
(60) Hales, D. A.; Lian, L.; Armentrout, P. B. Collision-Induced Dissociation of $Nb_n^+$ ($n$ = 2−11): Bond Energies and Dissociation Pathways. *Int. J. Mass Spectrom. Ion Processes* **1990**, *102*, 269−301.
(61) Armentrout, P. B.; Simons, J. Understanding Heterolytic Bond Cleavage. *J. Am. Chem. Soc.* **1992**, *114*, 8627−8633.
(62) Frisch, M. J.; Trucks, G. W.; Schlegel, H. B.; Scuseria, G. E.; Robb, M. A.; Cheeseman, J. R.; Scalmani, G.; Barone, V.; Mennucci, B.; Petersson, G. A.; Nakatsuji, H.; Caricato, M.; Li, X.; Hratchian, H. P.; Izmaylov, A. F.; Bloino, J.; Zheng, G.; Sonnenberg, J. L.; Hada, M.; Ehara, M.; Toyota, K.; Fukuda, R.; Hasegawa, J.; Ishida, M.; Nakajima, T.; Honda, Y.; Kitao, O.; Nakai, H.; Vreven, T.; Montgomery, J. A.; Peralta, J. E.; Ogliaro, F.; Bearpark, M.; Heyd, J. J.; Brothers, E.; Kudin, K. N.; Staroverov, V. N.; Kobayashi, R.; Normand, J.; Raghavachari, K.; Rendell, A.; Burant, J. C.; Millam, J. M.; Iyengar, S. S.; Tomasi, J.; Cossi, M.; Rega, N.; Millam, J. M.; Klene, M.; Knox, J. E.; Cross, J. B.; Bakken, V.; Adamo, C.; Jaramillo, J.; Gomperts, R.; Stratmann, R. E.; Yazyev, O.; Austin, A. J.; Cammi, R.; Pomelli, C.; Ochterski, J. W.; Martin, R. L.; Morokuma, K.; Zakrzewski, V. G.; Voth, G. A.; Salvador, P.; Dannenberg, J. J.; Dapprich, S.; Daniels, A. D.; Farkas, O.; Foresman, J. B.; Ortiz, J. V.; Cioslowski, J.; Fox, D. J. *Gaussian 09*, Revision A.02; Gaussian Inc.: Pittsburgh, PA, 2009.
(63) Becke, A. D. Density-functional Thermochemistry. III. The Role of Exact Exchange. *J. Chem. Phys.* **1993**, *98*, 5648−5652.
(64) Lee, C.; Yang, W.; Parr, R. G. Development of the Colle-Salvetti Correlation-Energy Formula into a Functional of the Electron Density. *Phys. Rev. B* **1988**, *37*, 785−789.
(65) Hay, P. J.; Wadt, W. R. Ab Initio Effective Core Potentials for Molecular Calculations. Potentials for K to Au Including the Outermost Core Orbitals. *J. Chem. Phys.* **1985**, *82*, 299−310.
(66) Glendening, E. D.; Feller, D.; Thompson, M. A. An Ab Initio Investigation of the Structure and Alkali Metal Cation Selectivity of 18-Crown-6. *J. Am. Chem. Soc.* **1994**, *116*, 10657−10669.
(67) Weigend, F.; Ahlrichs, R. Def2-SVP Basis Sets. *Phys. Chem. Chem. Phys.* **2005**, *7*, 3297−3305.
(68) Rappoport, D.; Furche, F. Property-Optimized Gaussian Basis Sets for Molecular Response Calculations. *J. Chem. Phys.* **2010**, *133*, 134105.
(69) Leininger, T.; Nicklass, A.; Kuechle, W.; Stoll, H.; Dolg, M.; Bergner, A. The Accuracy of the Pseudopotential Approximation: Non-Frozen-Core Effects for Spectroscopic Constants of Alkali Fluorides XF (X = K, Rb, Cs). *Chem. Phys. Lett.* **1996**, *255*, 274−280.
(70) Feller, D. The Role of Databases in Support of Computational Chemistry Calculations. *J. Comput. Chem.* **1996**, *17*, 1571−1586.
(71) Schuchardt, K. L.; Didier, B. T.; Elsethagen, T.; Sun, L.; Gurumoorthi, V.; Chase, J.; Li, J.; Windus, T. L. Basis Set Exchange: A Community Database for Computational Sciences. *J. Chem. Inf. Model.* **2007**, *47*, 1045−1052.
(72) Foresman, J. B.; Frisch, A. E. *Exploring Chemistry with Electronic Structure Methods*, 2nd ed.; Gaussian, Inc.: Pittsburgh, PA, 1996.
(73) Zhao, Y.; Truhlar, D. G. The M06 Suite of Density Functionals for Main Group Thermochemistry, Thermochemical Kinetics, Noncovalent Interactions, Excited States, and Transition Elements: Two New Functionals and Systematic Testing of Four M06-Class Functionals and 12 Other Functionals. *Theor. Chem. Acc.* **2008**, *120*, 215−241.
(74) Möller, C.; Plesset, M. S. Note on an Approximation Treatment for Many-Electron Systems. *Phys. Rev.* **1934**, *46*, 618−622.
(75) Boys, S. F.; Bernardi, R. The Calculation of Small Molecular Interactions by the Differences of Separate Total Energies. Some Procedures with Reduced Errors. *Mol. Phys.* **1970**, *19*, 553−566.
(76) van Duijneveldt, F. B.; van Duijneveldt-van de Rijdt, J. G. C. M.; van Lenthe, J. H. State of the Art in Counterpoise Theory. *Chem. Rev.* **1994**, *94*, 1873−1885.
(77) Heaton, A. L.; Ye, S. J.; Armentrout, P. B. Experimental and Theoretical Studies of Sodium Cation Complexes of the Deamidation and Dehydration Products of Asparagine, Glutamine, Aspartic Acid, and Glutamic Acid. *J. Phys. Chem. A* **2008**, *112*, 3328−3338.
(78) Heaton, A. L.; Armentrout, P. B. Thermodynamics and Mechanism of the Deamidation of Sodium-Bound Asparagine. *J. Am. Chem. Soc.* **2008**, *130*, 10227−10232.
(79) Lifshitz, C. Recent Developments in Applications of RRKM-QET. *Adv. Mass Spectrom.* **1989**, *11*, 713−729.
(80) Wilson, R. G.; Brewer, G. R. *Ion Beams with Applications to Ion Implantation*; Wiley: New York, 1973.
(81) Smith, S. M.; Markevitch, A. N.; Romanor, D. A.; Li, X.; Levis, R. J.; Schlegel, H. B. Static and Dynamic Polarizabilities of Conjugated Molecules and Their Cations. *J. Phys. Chem. A* **2000**, *108*, 11063−11072.